A theory of traffic congestion at heavy bottlenecks

2008 J. Phys. A: Math. Theor. 41 215101

(http://iopscience.iop.org/1751-8121/41/21/215101)

IOP PUBLISHING JOURNAL OF PHYSICS A: MATHEMATICAL AND THEORETICAL

J. Phys. A: Math. Theor. **41** (2008) 215101 (42pp) doi:10.1088/1751-8113/41/21/215101

A theory of traffic congestion at heavy bottlenecks

Boris S Kerner

Daimler AG, GR/ETI, HPC: G021, 71059 Sindelfingen, Germany

Received 28 February 2008, in final form 14 April 2008
Published 7 May 2008
Online at stacks.iop.org/JPhysA/41/215101

Abstract

Spatiotemporal features and physics of vehicular traffic congestion occurring due to heavy highway bottlenecks caused for example by bad weather conditions or accidents are found based on simulations in the framework of three-phase traffic theory. A model of a heavy bottleneck is presented. Under a continuous non-limited increase in bottleneck strength, i.e., when the average flow rate within a congested pattern allowed by the heavy bottleneck decreases continuously up to zero, the evolution of the traffic phases in congested traffic, synchronized flow and wide moving jams, is studied. It is found that at a small enough flow rate within the congested pattern, the pattern exhibits a non-regular structure: a pinch region of synchronized flow within the pattern disappears and appears randomly over time; wide moving jams upstream of the pinch region exhibit a complex non-regular dynamics in which the jams appear and disappear randomly. At greater bottleneck strengths, wide moving jams merge onto a mega-wide moving jam (mega-jam) within which low-speed patterns with a complex non-regular spatiotemporal dynamics occur. We show that when the bottleneck strength is great enough, only the mega-jam survives and synchronized flow remains only within its downstream front separating free flow and congested traffic. Theoretical results presented can explain why no sequence of wide moving jams can often be distinguished in non-homogeneous traffic congestion measured at very heavy bottlenecks caused by bad weather conditions or accidents.

PACS numbers: 89.40.+k, 47.54.+r, 64.60.Cn, 64.60.Lx

1. Introduction

The physics of freeway traffic congestion is one of the most quickly developed fields of complex spatiotemporal systems. In empirical observations, traffic breakdown (onset of congestion) in free flow occurs mostly at bottlenecks associated with, e.g., on- and off-ramps. In congested traffic, moving jams are observed [1–12]. A moving jam is a localized structure of great vehicle density, spatially limited by two jam fronts; the jam propagates upstream; within the jam vehicle speed is very low.

Moving jams, which exhibit a characteristic jam feature [J] to propagate through bottlenecks while maintaining the mean velocity of the downstream jam front, are called *wide* moving jams [12].

In observations [12], traffic breakdown is associated with a local first-order phase transition from free flow to synchronized flow (F → S transition) at the bottleneck; synchronized flow [S] is defined as congested traffic that does not exhibit the feature [J]; in particular, the downstream front of synchronized flow is often *fixed* at the bottleneck. Wide moving jams can emerge spontaneously in synchronized flow (S → J transition) only, i.e., due to a sequence of F → S → J transitions.

Moving jam emergence in synchronized flow leading to S → J transitions is called the pinch effect occurring within an associated pinch region of synchronized flow [12]: (i) The density increases and average speed decreases; narrow moving jams, which do not exhibit the feature [J], appear in the pinch region. (ii) These jams propagate upstream growing in their amplitude; as a result, S → J transitions occur, i.e., wide moving jams emerge. The upstream boundary of the pinch region is a road location at which a narrow moving jam has just transformed into a wide moving one. (iii) These locations can vary for different wide moving jams, i.e., the pinch region width (in the longitudinal direction) depends on time. A congested traffic pattern at an isolated bottleneck that exhibits this regular structure is called a general pattern (GP). The increase in density of synchronized flow with the subsequent emergence of growing narrow moving jams explains the terms *pinch effect* and *pinch region* of synchronized flow within the GP.

Earlier traffic flow theories and models reviewed in [1–10], which are associated with the so-called fundamental diagram approach to traffic flow modeling, cannot explain F → S → J transitions and the pinch effect (see a criticism of the theories in [12, 15]). For this reason, the author introduced a three-phase traffic theory (references in [12]) in which there are (i) the free flow, (ii) synchronized flow and (iii) wide moving jam phases. The synchronized flow and wide moving jam phases associated with congested traffic are defined via the empirical definitions [S] and [J], respectively. The first three-phase traffic flow models showing the pinch effect are stochastic microscopic models [16, 17]. Later, other three-phase traffic flow models were developed [15, 18–22]. Recent simulation results in the framework of the author's three-phase traffic theory can be found in [23–28].

The spatiotemporal criteria for a wide moving jam [J] can be explained by a traffic flow interruption that occurs when vehicles are in a standstill within the wide moving jam. A sufficient criterion for this flow interruption within the jam is [13, 14]

$$I_s = \frac{\tau_{max}}{\tau_{del}^{(ac)}} \gg 1, \tag{1}$$

where τ_{max} is the maximum time headway between two vehicles within a wide moving jam and $\tau_{del}^{(ac)}$ is the mean time delay in vehicle acceleration at the downstream jam front from a vehicle standstill; $\tau_{del}^{(ac)}$ determines the jam outflow; corresponding to empirical results $\tau_{del}^{(ac)} \approx 1.5$ –2 s [12].[1] The *flow interruption effect* is a general effect for each wide moving jam. For this reason, criterion (1) can be considered as a microscopic criterion for the wide moving jam phase. If a congested traffic state is not related to the wide moving jam phase, i.e., criterion (1) is not satisfied, then with certainty the state is associated with the synchronized flow phase.

[1] At a given time instant $t = t_1$, the time headway (time gap) between vehicles $\tau(t_1)$ is *defined* as a time it takes for a vehicle to reach a freeway location at which the bumper of the preceding vehicle is at the time instant t_1. In single-vehicle data measured at a road detector, t_1 is the time at which the preceding vehicle leaves the detector whose location is therefore related to the location of the bumper of the preceding vehicle in the time headway definition; the time headway is equal to $\tau(t_1) = t_2 - t_1$, where t_2 is the time at which the vehicle front has been recorded at the detector.

This is because congested traffic can be either within the synchronized flow phase or within the wide moving jam phase. In numerical simulations has been found [14] that if in (1) $I_s > 5$, then a moving jam propagates through a bottleneck, i.e., this jam is a wide moving one.

In general, the average flow rate $q^{(\mathrm{cong})}$ within a congested traffic pattern upstream of a bottleneck is the smaller, the greater the bottleneck influence of traffic (called the bottleneck strength). The time interval of the averaging of the flow rate $q^{(\mathrm{cong})}$ is suggested to be considerably longer than time distances between any moving jams within a congested pattern. Empirical data show that the flow rate $q^{(\mathrm{cong})}$ within GPs occurring at usual bottlenecks like on- and off-ramp bottlenecks, which is equal to the average flow rate in the pinch region $q^{(\mathrm{pinch})}$, is approximately within a range

$$q^{(\mathrm{cong})} = q^{(\mathrm{pinch})} = 1100\text{–}1700 \text{ vehicles/h/lane}. \tag{2}$$

Features of GPs and other congested patterns occurring at usual bottlenecks determined by road infrastructure (on- and off-ramps, road gradients, etc), for which condition (2) is valid, have already been studied in detail [12]. In contrast with the usual bottlenecks, due to for example bad weather conditions or accidents highway bottlenecks can occur, which exhibit a much greater influence on traffic (greater bottleneck strength) that limits $q^{(\mathrm{cong})}$ to very *small* values, sometimes as low as zero, when condition (2) is not satisfied. Such a bottleneck can be called a *heavy bottleneck*. Features of traffic congestion at heavy bottlenecks are unknown.

Some suggestions about these features can already be made from the following qualitative consideration. Recent empirical studies of sequences of wide moving jams [13, 14] show that in empirical data between flow interruption intervals, vehicles within a wide moving jam exhibit time headways about 1.5–7 s [14]. These time headways are considerably shorter than flow interruption intervals ($\tau_{\max} > 10$ s, i.e., $I_s > 5$ in (1)). When vehicles meet the wide moving jam, firstly they decelerate at the upstream jam front to a standstill. Space gaps between these vehicles can be very different, i.e., blanks (regions with no vehicles) can appear within the jam. Later vehicles move covering these blanks. Consequently, due to this low-speed vehicle motion new blanks between vehicles occur upstream, i.e., *moving blanks* appear propagating upstream within the jam. In measured data, the average flow rate within wide moving jams $q^{(\mathrm{blanks})}$ caused by a low-speed vehicle motion within the jams associated with moving blanks satisfies an approximate condition

$$q^{(\mathrm{blanks})} \lesssim 600 \text{ vehicles/h/lane}. \tag{3}$$

The average flow rate within wide moving jams $q^{(\mathrm{blanks})}$ is defined as a number of vehicles $N^{(\mathrm{blanks})}$, which have passed a virtual road detector during time intervals of the propagation of n_J wide moving jams (it is assumed that $n_J \gg 1$) through the detector, divided by the sum of these time intervals,

$$q^{(\mathrm{blanks})} = \frac{N^{(\mathrm{blanks})}}{\sum_{i=1}^{n_J} \tau_J^{(i)}}, \tag{4}$$

where $\tau_J^{(i)}$ is a duration of a ith wide moving jam, i.e., the time interval between the downstream and upstream fronts of the jam i, while this jam propagates through the detector.

Between the wide moving jams, the average flow rate associated with non-interrupted flows in the jam outflows $q_{\mathrm{out}}^{(\mathrm{J})}$ is greater than $q^{(\mathrm{pinch})}$ (2), i.e., $q_{\mathrm{out}}^{(\mathrm{J})}$ is considerably greater than $q^{(\mathrm{blanks})}$ (3). Now we assume that due to bad weather conditions or an accident a heavy bottleneck occurs with a great strength for which

$$q^{(\mathrm{cong})} = q^{(\mathrm{blanks})}. \tag{5}$$

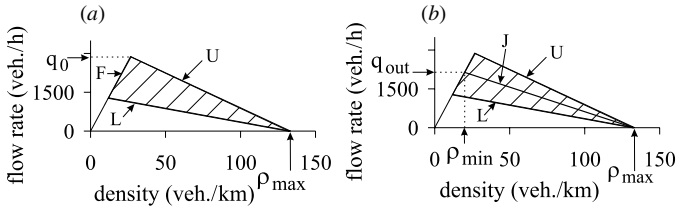

Figure 1. Steady speed states for the Kerner–Klenov stochastic three-phase traffic flow in the flow-density plane (*a*) and the line J (*b*). Taken from [12].

In this case, $q_{\text{out}}^{(\text{J})}$ must reduce to $q^{(\text{blanks})}$ (3), i.e., the difference between flows within and outside wide moving jams disappears. As a result, at

$$q^{(\text{cong})} \leqslant q^{(\text{blanks})} \tag{6}$$

wide moving jams should merge into a mega-wide moving jam (mega-jam for short). Thus already from this qualitative consideration, we can expect interesting physical phenomena associated with the complexity of traffic congestion at heavy bottlenecks.

In this paper, we reveal these phenomena. The paper is organized as follows. In section 2, we discuss a stochastic three-phase traffic flow model of [16, 29] as well as present a heavy bottleneck model used for simulations of traffic congestion. A theory of the evolution of traffic phases at heavy bottlenecks is presented in section 3. A microscopic spatiotemporal non-regular dynamics of wide moving jams is presented in section 4. In section 5, a microscopic spatiotemporal structure and dynamics of mega-jams are presented. An explanation of features of traffic congestion at heavy bottlenecks found in sections 3–5 and a comparison of the theoretical results with some measured traffic data as well as a summary of the key results are made in section 6.

2. Model of road with heavy bottleneck

2.1. Two-lane stochastic three-phase traffic flow model

For a theoretical analysis of traffic congestion at heavy bottlenecks, we use a stochastic three-phase traffic flow model of a two-lane road [16, 29]. Basic driver behavioral assumptions of this Kerner–Klenov model are as follows:

(i) *Fundamental hypothesis of three-phase traffic theory* [12]. In synchronized flow, a driver accepts a range of different hypothetical steady state speeds at the same space gap to the preceding vehicle. This means that hypothetical steady model states of synchronized flow cover a 2D-region in the flow-density plane (figure 1(*a*)). The boundaries of this 2D-region F, L and U are respectively associated with free flow, a synchronization space gap, and a safe space gap determined through a safe speed. The 2D-region of steady states is associated with a driver behavioral assumption that in synchronized flow a driver is able to recognize whether the space gap is increasing or deceasing regardless of the speed difference to the preceding vehicle.

(ii) *Line J and 2D-region of steady states* [12]. In the model, the line J, which represents in the flow-density plane the steady propagation of the downstream front of a wide moving jam (the slope of the line J is equal to the mean velocity of this jam front) [12], is between the boundaries L and U (figure 1(*b*)), i.e., the line J divides the 2D-region of steady states of synchronized flow onto two classes: the states on and above the line J and the states

below the line J, which are metastable and stable states with respect to wide moving jam formation, respectively. Thus at a given steady speed, a driver behavioral assumption is that the space gap in synchronized flow associated with the line J, i.e., in the jam outflows is greater than the safe gap and it is smaller than the synchronization gap.

(iii) *Speed adaptation effect in synchronized flow* [12]. The speed adaptation effect takes place when the vehicle cannot pass the preceding vehicle, within the space gap range

$$g_{\mathrm{s,n}} \leqslant g_n \leqslant G_n, \tag{7}$$

where $g_n = x_{\ell,n} - x_n - d$ is the space gap, x_n is the vehicle co-ordinate, the lower index ℓ marks functions and values related to the preceding vehicle; $g_{\mathrm{s,n}}$ is the safe space gap determined from the equation $v_{\mathrm{n}} = v_{\mathrm{s,n}}$, in which v_{n} is the vehicle speed, $v_{\mathrm{s,n}}$ is a safe speed; G_n is a synchronization space gap; all vehicles have the same length d, which includes the minimum space gap between vehicles within a wide moving jam; index n corresponds to the discrete time $t = n\tau$, $n = 0, 1, 2, \ldots$; τ is time step. Under condition (7), the vehicle tends to adjust its speed to the preceding vehicle without caring, what the precise space gap is, as long as it is safe. For example, at a given time-independent speed of the preceding vehicle $v_{\ell,n} = v_\ell = \mathrm{const}$, this speed adaptation leads to car following with $v_n = v = v_\ell$ at a time-independent space gap $g_n = g$. There is an infinite number of these gaps associated with the same speed $v = v_\ell$. These gaps lie between the synchronization gap and safe gap, i.e., there is no desired (or optimal) space gap in synchronized flow.

(iv) *Over-acceleration effect* [12]. In synchronized flow of a lower density, a driver searches for the opportunity to accelerate and to pass. A competition between the speed adaptation (item (iii)) and over-acceleration effects simulates traffic breakdown (F $\rightarrow$ S transition). The over-acceleration is simulated as a collective effect, which occurs on average in traffic flow, through the use of random vehicle acceleration

$$\xi_{\mathrm{a}} = a\tau\Theta(p_{\mathrm{a}} - r), \tag{8}$$

where p_{a} is probability of random acceleration, a is the maximum acceleration, $r = \mathrm{rand}(0, 1)$, $\Theta(z) = 0$ at $z < 0$ and $\Theta(z) = 1$ at $z \geqslant 0$. The model fluctuations (8) are applied only if the vehicle should accelerate without model fluctuations.

(v) *Pinch effect in synchronized flow* [12]. Moving in synchronized flow, a driver comes on average closer to the preceding vehicle over time that should explain the pinch effect. A driver time delay in deceleration simulates this effect through model fluctuations in deceleration

$$b_n = a\Theta(P_{\mathrm{l}} - r_{\mathrm{l}}), \tag{9}$$

applied under condition (7) only; P_{l} is probability of random deceleration, $r_{\mathrm{l}} = \mathrm{rand}(0, 1)$.

(vi) *Over-deceleration effect*. As in the Nagel–Schreckenberg (NaSch) cellular automata CA model [30], a well-known over-deceleration effect (human over-reaction) associated with driver reaction time [31] is also simulated as a collective effect through the use of random fluctuations in vehicle deceleration

$$\xi_{\mathrm{b}} = a\tau\Theta(p_{\mathrm{b}} - r), \tag{10}$$

which is applied only if the vehicle should decelerate without model fluctuations; p_{b} is the probability of random deceleration. In the Kerner–Klenov model, a competition between the over-deceleration and the speed adaptation effect (item (iii)) determines moving jam emergence in synchronized flow.

(vii) *Driver time delay in acceleration.* In the model, this well-known effect should describe driver delay in acceleration at the downstream front of synchronized flow or wide moving jam (in the latter case, the driver delay in acceleration is known as a slow-to-start rule [32]) after the preceding vehicle has begun to accelerate. A driver time delay in acceleration is simulated as a collective effect through the use of a random value of vehicle acceleration

$$a_n = a\Theta(P_0 - r_1) \tag{11}$$

applied under condition (7) and only then if the vehicle did not accelerate at the former time step; in the latter case $P_0 = p_0 > 0$, i.e., a vehicle accelerates with some probability p_0 that depends on the speed v_n; otherwise $P_0 = 0$. As in the NaSch CA model [32], the mean time in vehicle acceleration is

$$\tau_{\mathrm{del}}^{(\mathrm{a})} = \frac{\tau}{1 - p_0}. \tag{12}$$

Thus, the basis of the Kerner–Klenov stochastic three-phase traffic flow model are driver behavioral assumptions made in three-phase traffic theory (items (i)–(v)) [12]. In addition, over-deceleration (item (vi)) and driver time delay in acceleration (item (vii)) introduced in earlier traffic flow models in the framework of the fundamental diagram approach have also been incorporated; in particular, as in the NaSch CA model [30, 32], these driver time delays appear through the use of model fluctuations. Finally, the Kerner–Klenov stochastic three-phase traffic flow model reads as follows:

$$v_{n+1} = \max(0, \min(v_{\mathrm{free}}, \tilde{v}_{n+1} + \xi_n, v_n + a\tau, v_{\mathrm{s},n})), \tag{13}$$

$$x_{n+1} = x_n + v_{n+1}\tau, \tag{14}$$

$$\tilde{v}_{n+1} = \max(0, \min(v_{\mathrm{free}}, v_{\mathrm{c},n}, v_{\mathrm{s},n})), \tag{15}$$

$$v_{c,n} = \begin{cases} v_n + \Delta_n & \text{at} \quad g_n \leqslant G_n \\ v_n + a_n\tau & \text{at} \quad g_n > G_n, \end{cases} \tag{16}$$

where

$$\Delta_n = \max(-b_n\tau, \min(a_n\tau, v_{\ell,n} - v_n)), \tag{17}$$

with v_{free} being the maximum speed in free flow that is constant.

The synchronization gap G_n depends on the vehicle speed v_n and on the speed of the preceding vehicle $v_{\ell,n}$

$$G_n = G(v_n, v_{\ell,n}), \tag{18}$$

where the function $G(u, w)$ is chosen as

$$G(u, w) = \max(0, k\tau u + \phi_0 a^{-1} u(u - w)), \tag{19}$$

$k > 1$ and ϕ_0 are constants. If $v_n = v_{\ell,n}$, the synchronization gap G_n is $kv_n\tau$; this corresponds to a fixed time gap $k\tau$ that determines the line L in figure 1. If $v_n > v_{\ell,n}$, the gap G_n increases and vice versa.

As explained in items (iv) and (vi), random deceleration and acceleration ξ_n in (13) are applied depending on whether the vehicle decelerates or accelerates, or else maintains its speed,

$$\xi_n = \begin{cases} -\xi_{\mathrm{b}} & \text{if} \quad S_{n+1} = -1 \\ \xi_{\mathrm{a}} & \text{if} \quad S_{n+1} = 1 \\ 0 & \text{if} \quad S_{n+1} = 0, \end{cases} \tag{20}$$

where S in (20) denotes the state of motion ($S_{n+1} = -1$ represents deceleration, $S_{n+1} = 1$ acceleration, and $S_{n+1} = 0$ motion at nearly constant speed)

$$S_{n+1} = \begin{cases} -1 & \text{if} \quad \tilde{v}_{n+1} < v_n - \delta \\ 1 & \text{if} \quad \tilde{v}_{n+1} > v_n + \delta \\ 0 & \text{otherwise,} \end{cases} \tag{21}$$

where δ is constant ($\delta \ll a\tau$).

In (11) and (9), the probabilities P_0 and P_1 are

$$P_0 = \begin{cases} p_0(v_n) & \text{if} \quad S_n \neq 1 \\ 1 & \text{if} \quad S_n = 1, \end{cases} \tag{22}$$

$$P_1 = \begin{cases} p_1 & \text{if} \quad S_n \neq -1 \\ p_2(v_n) & \text{if} \quad S_n = -1, \end{cases} \tag{23}$$

where speed functions for probabilities $p_0(v_n)$ and $p_2(v_n)$ are considered in [12]; p_1 is constant.

The safe speed $v_{s,n}$ in (13) is chosen in the form

$$v_{s,n} = \min\left(v_n^{(\text{safe})}, g_n/\tau + v_\ell^{(a)}\right), \tag{24}$$

where $v_n^{(\text{safe})} = v^{(\text{safe})}(g_n, v_{\ell,n})$ [33] is a solution of the Gipps equation [34]

$$v^{(\text{safe})}\tau^{(\text{safe})} + X_d(v^{(\text{safe})}) = g_n + X_d(v_{\ell,n}), \tag{25}$$

where $\tau^{(\text{safe})}$ is a safety time headway (safety time gap) to the preceding vehicle, $X_d(u)$ is the distance traveled by the vehicle with an initial speed u at a time-independent deceleration b until it comes to a stop; $v_\ell^{(a)}$ is an 'anticipation' speed of the preceding vehicle at the next time step (formula (16.48) of [12]).

The following incentive conditions for lane changing from the right lane to the left lane ($R \to L$) and a return change from the left lane to the right lane ($L \to R$) have been used in the model:

$$R \to L : v_n^+ \geqslant v_{\ell,n} + \delta_1 \qquad \text{and} \quad v_n \geqslant v_{\ell,n}, \tag{26}$$

$$L \to R : v_n^+ > v_{\ell,n} + \delta_1 \qquad \text{or} \quad v_n^+ > v_n + \delta_1. \tag{27}$$

The security conditions for lane changing are given by the inequalities:

$$g_n^+ > \min\left(v_n\tau, G_n^+\right), \tag{28}$$

$$g_n^- > \min\left(v_n^-\tau, G_n^-\right), \tag{29}$$

where

$$G_n^+ = G\left(v_n, v_n^+\right), \tag{30}$$

$$G_n^- = G\left(v_n^-, v_n\right), \tag{31}$$

the function $G(u, w)$ is given by (19); the speed v_n^+ or the speed $v_{\ell,n}$ in (28), (29) is set to ∞ if the space gap g_n^+ or the space gap g_n exceeds a given look-ahead distance L_a, respectively; superscripts + and − in variables, parameters and functions denote the preceding vehicle and the trailing vehicle in the 'target' (neighboring) lane, respectively. The target lane is the lane into which the vehicle wants to change. If the conditions (26)–(29) are satisfied, the vehicle changes lanes with probability p_c. p_c, δ_1 ($\delta_1 \geqslant 0$), L_a are constants. These and other model parameters in all simulations presented below are listed in table 16.11 of the book [12].

2.2. Model of heavy bottleneck

To describe a heavy bottleneck, we suggest that there is a section of the road of a length $L_{\rm B}$ within which due to an accident or bad weather conditions drivers should increase a safety time headway $\tau^{(\rm safe)}$ to the preceding vehicle as well as decrease the maximum speed to some $v_{\rm B}$ that is lower than the maximum speed in free flow $v_{\rm free}$: within the section, the safety time headway is equal to $\tau^{(\rm safe)} = T_{\rm B} > 1$ s that is longer than $\tau^{(\rm safe)} = 1$ s used in the model for vehicles moving outside this section.

In according with equation (25) of the model, $\tau^{(\rm safe)}$ determines a safe speed, which should not be exceeded by a driver; otherwise, the driver decelerates. As a result, within this section drivers move with the mean time headway that is longer than the mean time headway outside the bottleneck section and it is the longer, the longer $\tau^{(\rm safe)} = T_{\rm B}$. Therefore the section with longer $\tau^{(\rm safe)} = T_{\rm B}$ acts as a bottleneck on the road. In the bottleneck model, at given $L_{\rm B}$ and $v_{\rm B}$ each chosen value $T_{\rm B}$ defines a specific bottleneck: the strength of this bottleneck is the greater, the longer $T_{\rm B}$; in turn, the longer $T_{\rm B}$, the smaller $q^{(\rm cong)}$, i.e., the greater the flow rate limitation within congestion caused by the bottleneck.

This model feature allows us to simulate a heavy bottleneck caused by bad weather conditions or accidents leading to a long enough $T_{\rm B}$ within the bottleneck, i.e., to a great bottleneck strength. Under bad weather conditions, a road section with a long value $T_{\rm B}$ can be caused, e.g., by a poor view due to fog on the section or a much longer deceleration way needed by snow and ice on the section. If an accident occurs on a road, a road section with a long value $T_{\rm B}$ can be caused, e.g., by much narrower lane widths allowed for driving on the road section; the same effect can occur under heavy roadworks.

In simulations discussed in below, we consider traffic phenomena occurring when the bottleneck strength increases gradually through the increase in $T_{\rm B}$, when other bottleneck parameters are given constants (figure 2). However as simulations show, at a given $T_{\rm B}$ the increase in $L_{\rm B}$ or/and decrease in $v_{\rm B}$ lead also to an increase in the bottleneck strength with the subsequent decrease in the average flow rate $q^{(\rm cong)}$ in congested traffic upstream of the bottleneck. For this reason, numerical values of $T_{\rm B}$ mentioned below, at which characteristic traffic phenomena occur at a heavy bottleneck, depend on $L_{\rm B}$ and $v_{\rm B}$. In contrast, we find that numerical values of the flow rate $q^{(\rm cong)}$ at which the traffic phenomena occur at the bottleneck do not change appreciably, when a greater value of $L_{\rm B}$ or/and another value of $v_{\rm B}$ (in the range 50–80 km h^{-1}) are chosen. For this reason, the flow rates $q^{(\rm cong)}$ can be considered characteristic values representing the bottleneck strength at given parameters of the Kerner–Klenov model used in simulations (section 2.1).

3. Traffic phases in congested traffic at heavy bottlenecks

When the bottleneck strength is not great, i.e., $T_{\rm B}$ is chosen to be not very long ($T_{\rm B} = 1.8$ s), then at a great enough flow rate $q_{\rm in}$ in free flow upstream of the bottleneck, firstly synchronized flow occurs spontaneously at the bottleneck. Then the pinch region with a relatively great flow rate $q^{(\rm cong)} = q^{(\rm pinch)}$ is formed (figures 2(*a*) and 3). At the pinch region upstream boundary wide moving jams emerge. Thus we found known phenomena of regular GP formation (figures 2(*a*) and 4(*a*), (*b*)) [12][2]. The pinch region width $L^{(\rm pinch)}(t)$ changes over time between about 1 km and 2 km (figure 5(*a*)). $L^{(\rm pinch)}$ is defined as the distance between the upstream boundary of the bottleneck ($x = 16$ km) and the road location upstream at which a wide moving jam has just been identified through the use of the jam microscopic criterion (1). There is also a nearly constant frequency of $L^{(\rm pinch)}(t)$ oscillations associated

[2] At $T_{\rm B} < 1.5$ s, rather than GPs, synchronized flow patterns (SP) are realized upstream of the bottleneck [12].

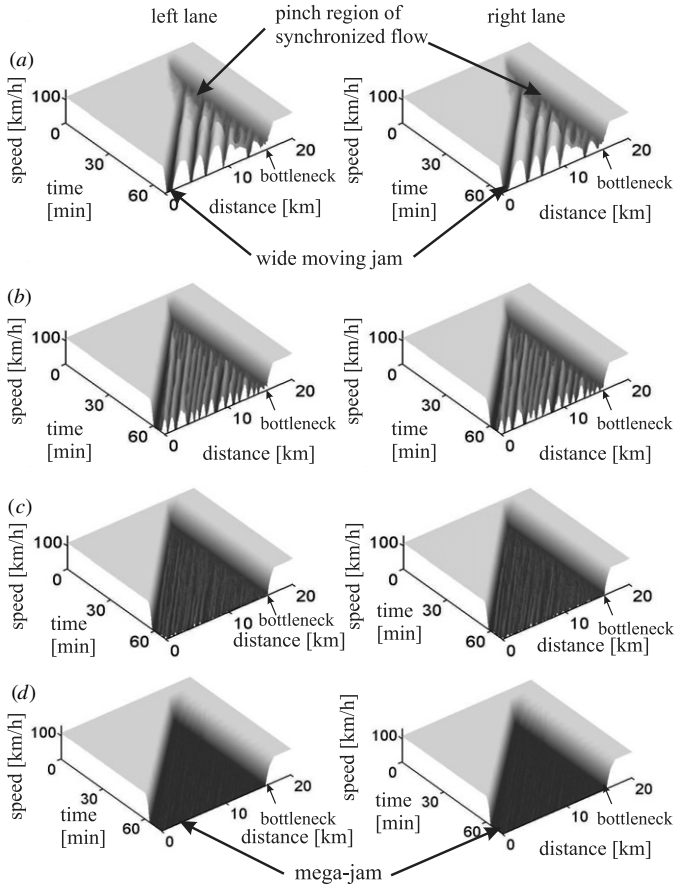

Figure 2. Simulated speed in space and time in the left (figures left) and right (right) road lanes at different T_B: $T_B = 1.8$ (*a*), 2.4 (*b*), 12 (*c*), 60 s (*d*). $q_{in} = 1946$ vehicles/h/lane. The upstream boundary of bottleneck region of the length $L_B = 300$ m is at $x = 16$ km; the maximum speed within this bottleneck region is $v_B = 60$ km h^{-1}. Resulting values of $q^{(cong)} = 1546$ (*a*), 1114 (*b*), 440 (*c*), 127 vehicles/h/lane (*d*).

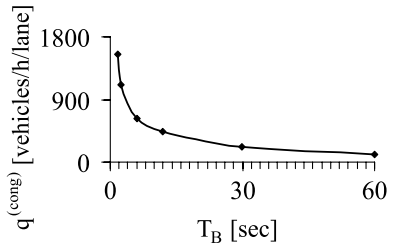

Figure 3. Simulated average flow rate $q^{(cong)}$ within congested patterns shown in figure 2 as a function of T_B. The averaging time interval for $q^{(cong)}$ is 60 min.

with the maximum in the Fourier spectrum (figure 5(*b*)). Speed autocorrelation functions and associated Fourier spectra of speed time dependencies at shorter T_B show regular character of wide moving jam propagation (figure 4(*c*), (*d*)).

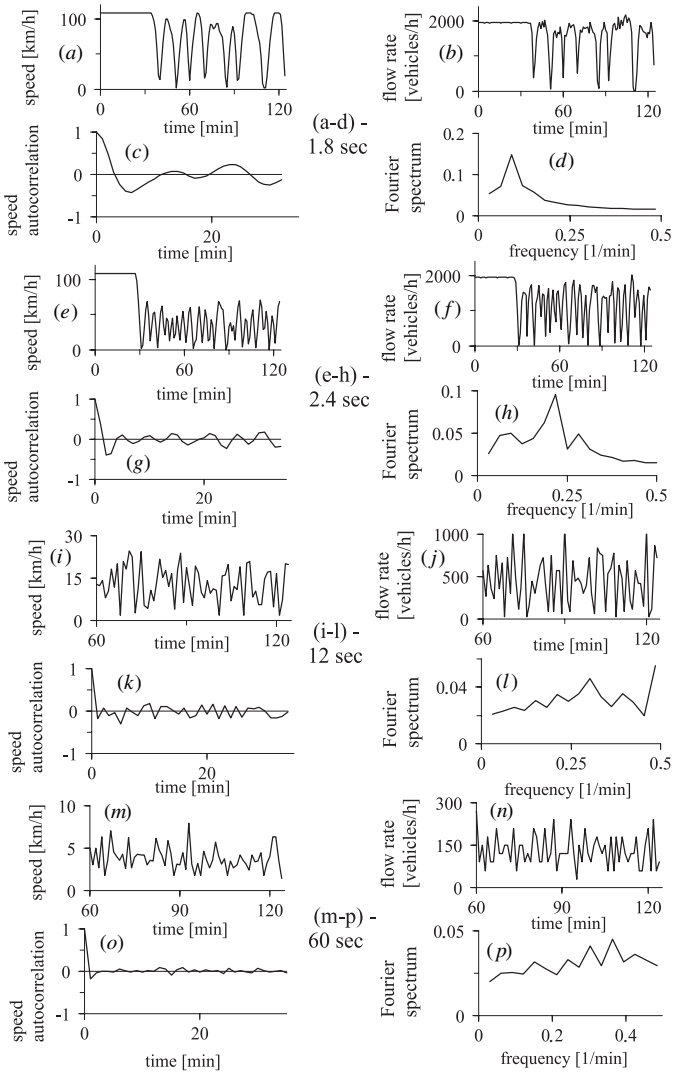

Figure 4. Simulated characteristics of congested patterns shown in figure 2 related to location 10 km. Time-functions of speed ((*a*), (*e*), (*i*), (*m*)), speed correlations ((*c*), (*g*), (*k*), (*o*)), associated Fourier spectra ((*d*), (*h*), (*l*), (*p*)) and flow rate ((*b*), (*f*), (*j*), (*n*)) for different $T_{\mathrm{B}} = 1.8$ (*a*)–(*d*), 2.4 (*e*)–(*h*), 12 (*i*)–(*l*), 60 s (*m*)–(*p*). 1 min average data in the left lane.

When T_{B} becomes longer and therefore the bottleneck strength increases, the flow rate $q^{(\mathrm{cong})} = q^{(\mathrm{pinch})}$ decreases (figure 3). However, if T_{B} remains a relatively small value ($1.8 < T_{\mathrm{B}} < 3$ s), then as for other bottleneck types, we found the following known GP features [12]: the smaller the flow rate $q^{(\mathrm{pinch})}$, the greater the frequency of narrow moving jam emergence within the pinch region, the lower the maximum (and the average) speed between wide moving jams upstream of the pinch region, the smaller the mean pinch region width $L_{\mathrm{mean}}^{(\mathrm{pinch})}$ (figures 2(*b*) and 5(*c*), (*d*), (*k*), (*l*)). This can also be seen from a comparison of time dependences of average speed within the region of wide moving jams for different T_{B} (figure 4(*a*), (*e*)).

Qualitatively other phenomena are found when $T_{\rm B}$ further increases ($T_{\rm B} > 3$ s) and the average flow rate $q^{(\rm cong)}$ decreases considerably (figures 2(*c*), (*d*) and 3).

We find that there is a critical strength of a heavy bottleneck associated with $T_{\rm B} = T_{\rm B}^{(\rm break)}$ that results in the critical flow rate $q^{(\rm cong)} = q_{\rm break}^{(\rm cong)}$. When

$$q^{(\rm cong)} \leqslant q_{\rm break}^{(\rm cong)} \tag{32}$$

related to $T_{\rm B} \geqslant T_{\rm B}^{(\rm break)}$, then there are random time intervals when the pinch region disappears, i.e., $L^{(\rm pinch)} = 0$ (figure 2(*e*), (*g*)). This means that there are time instants at which there is no pinch region and wide moving jams emerge directly at the upstream boundary of the bottleneck, whereas for other time intervals the pinch region appears again (figure 5(*e*), (*g*)). We found that $q_{\rm break}^{(\rm cong)} \approx 920$ vehicles/h/lane ($T_{\rm B}^{(\rm break)} \approx 3$ s at the chosen $L_{\rm B}$ and $v_{\rm B}$, see the caption to figure 2)[3]. Under condition (32), $L^{(\rm pinch)}(t)$ becomes a non-regular time-function (figure 5(*e*), (*g*), (*i*)) whose Fourier spectrum is the broader, the longer $T_{\rm B}$, i.e., the smaller $q^{(\rm cong)}$ (figure 5 (*f*), (*h*), (*j*)). Such a GP at an isolated heavy bottleneck can be considered the GP with a non-regular pinch region.

The more the bottleneck strength exceeds the critical bottleneck strength, the greater the difference $q_{\rm break}^{(\rm cong)} - q^{(\rm cong)}$ and the longer the mean duration of time intervals within which the regular structure of the GP breaks and the pinch region disappears, and therefore, the smaller the mean length $L_{\rm mean}^{(\rm pinch)}$ of the pinch region (figure 5 (*k*), (*l*)). In contrast with regular time dependences of the average speed within a sequence of wide moving jams (figure 4(*a*)–(*h*)), the time-functions of 1 min average speed at a greater bottleneck strength exhibit a non-regular behavior (figure 4(*i*)–(*l*)). This can be seen from speed autocorrelation functions and associated Fourier spectra of the average speed time dependences (figure 4(*k*), (*l*)).

When the bottleneck strength increases further, $L_{\rm mean}^{(\rm pinch)}$ decreases continuously (figure 5 (*k*), (*l*)). $L_{\rm mean}^{(\rm pinch)}$ reaches zero at a threshold bottleneck strength for the pinch region existence associated with $T_{\rm B} = T_{\rm B}^{(\rm th)}$ that results in a threshold flow rate $q^{(\rm cong)} = q_{\rm th}^{(\rm cong)}$. When

$$q^{(\rm cong)} \leqslant q_{\rm th}^{(\rm cong)} \tag{33}$$

related to $T_{\rm B} \geqslant T_{\rm B}^{(\rm th)}$, then the pinch region of GPs does not exist. At model parameters, the pinch region of an GP disappears fully at $q_{\rm th}^{(\rm cong)} \approx 220$ vehicles/h/lane ($T_{\rm B}^{(\rm th)} \approx 30$ s at the chosen $L_{\rm B}$ and $v_{\rm B}$).

There is also another critical bottleneck strength, which we call the critical bottleneck strength for the mega-jam formation associated with $T_{\rm B} = T_{\rm B}^{(\rm mega)}$ that results in the critical flow rate $q^{(\rm cong)} = q_{\rm mega}^{(\rm cong)}$. When

$$q^{(\rm cong)} \leqslant q_{\rm mega}^{(\rm cong)} \tag{34}$$

related to $T_{\rm B} \geqslant T_{\rm B}^{(\rm mega)}$, then wide moving jams *merge* onto a mega-jam. Numerical simulations show that (34) is equivalent to (6), i.e.,

$$q_{\rm mega}^{(\rm cong)} = q^{(\rm blanks)}. \tag{35}$$

At model parameters, $q_{\rm mega}^{(\rm cong)} \approx 130$ vehicles/h/lane ($T_{\rm B}^{(\rm mega)} \approx 60$ s at the chosen $L_{\rm B}$ and $v_{\rm B}$).

[3] It should be noted that $q_{\rm break}^{(\rm cong)}$ exhibits a probabilistic behavior: it is characterized by a given probability that the regular structure of an GP breaks at least one time during a given time interval $T_{\rm ob}$ for observing congested traffic. The mentioned value $q_{\rm break}^{(\rm cong)}$ is related to simulation results that with the probability, which is equal to one, a wide moving jam emerges whose upstream front is between road locations $16 \geqslant x > 15.95$ km (the pinch region width is smaller than 50 m at least for one time interval), i.e., the regular structure of an GP breaks at least one time in each of the 30 simulation runs made at the same model parameters during $T_{\rm ob} = 120$ min. For $T_{\rm ob} = 60$–120 min associated with the duration of traffic congestion in real traffic, at the chosen model parameters the dependence $q_{\rm break}^{(\rm cong)}(T_{\rm ob})$ is weak and it changes none of the qualitative results of the paper.

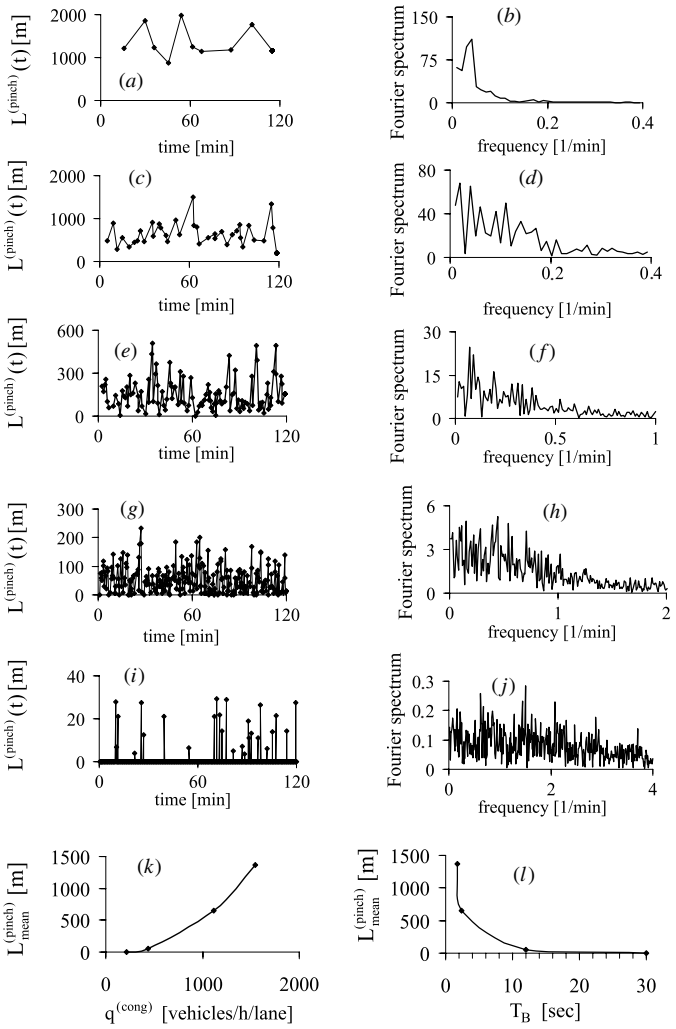

Figure 5. Simulations of pinch effect: $L^{(\mathrm{pinch})}(t)$ ((*a*), (*c*), (*e*), (*g*), (*i*)), associated Fourier spectra ((*b*), (*d*), (*f*), (*h*), (*j*)) for congested patterns related to $T_B = 1.8$ ((*a*), (*b*)), 2.4 ((*c*), (*d*)), 6 ((*e*), (*f*)), 12 ((*g*), (*h*)) and 30 s ((*i*), (*j*)). ((*k*), (*l*)) $L^{(\mathrm{pinch})}_{\mathrm{mean}}(q^{(\mathrm{cong})})$ (k) and $L^{(\mathrm{pinch})}_{\mathrm{mean}}(T_B)$ (l). For $T_B = 6$ and 30 s, $q^{(\mathrm{cong})} = 626$ and 218 vehicles/h/lane, respectively.

We found also that the critical bottleneck strength for the mega-jam formation is greater than the threshold bottleneck strength for the pinch region existence that results in the condition

$$q_{\mathrm{mega}}^{(\mathrm{cong})} < q_{\mathrm{th}}^{(\mathrm{cong})} \tag{36}$$

related to $T_B^{(\mathrm{mega})} > T_B^{(\mathrm{th})}$. Under condition (34), i.e., when all wide moving jams merge onto a mega-jam, traffic congestion upstream of an isolated heavy bottleneck cannot be considered as an GP any more. Thus in accordance with (34), (35), if traffic breakdown has occurred at a bottleneck, then the condition

$$q^{(\mathrm{cong})} > q^{(\mathrm{blanks})} \tag{37}$$

is a *necessary* condition for GP existence at this bottleneck.

As for GPs with a very non-regular pinch region (figure 4(*i*)–(*l*)), the time-functions of 1 min average speed within the mega-jam exhibit a non-regular behavior (figure 4(*m*)); this can be seen from speed autocorrelation functions and associated Fourier spectra of the average speed time dependences (figure 4(*o*), (*p*)).

When $q^{(\mathrm{cong})}$ becomes zero, because behind a road location the road is closed, the mega-jam transforms into a queue of *motionless* vehicles, which therefore is not associated with vehicular traffic. Nevertheless, there is a link between the queue and the mega-jam. If at a time instant we allow several vehicles to escape from this queue, then simulations show that motion of these vehicles results in wide moving jam occurrence, if the number of escaping vehicles is chosen to be great enough: the downstream front of the jam separates moving vehicles escaping from the queue and vehicles standing within the queue upstream of the front. When the number of vehicles, which are allowed to escape from the initial queue of motionless vehicles, decreases considerably, the downstream jam front transforms into a moving blank(s) subsequently covered by vehicles standing in the queue. When a vehicle per a long enough time interval is allowed to escape from the mega-jam, as simulations show, a sequence of such moving blanks within this jam occur; these moving blanks exhibit, however, the dynamics specifically associated with the mega-jam (section 5).

Thus based on a study of three-phase traffic flow model we found that the complexity of traffic congestion at a heavy bottleneck caused for example by bad weather conditions or accidents is associated with the phenomenon of random disappearance and appearance of the pinch region over time as well as with the phenomenon of the merger of wide moving jams into a mega-jam. When the bottleneck strength increases continuously, the mean length of the pinch region decreases also continuously up to zero; at such a heavy bottleneck, the pinch region does not exist any more. Beginning from a greater bottleneck strength only the mega-jam survives in congested traffic upstream of the bottleneck and synchronized flow remains only within its downstream front separating free flow and congested traffic. In other words, in congested traffic occurring at such a very heavy bottleneck there are no continuous flows within the congested pattern any more with the one exception of the downstream front of synchronized flow that separates free flow downstream and the mega-jam upstream of the front. Synchronized flow remains *only* within this front. These phenomena reveal the evolution of the traffic phases in congested traffic when heavy bottlenecks occur in highway traffic.

4. Microscopic spatiotemporal features of non-regular moving jam dynamics

4.1. Non-regular pinch region of general patterns

For GPs with a regular pinch region ((32) is not satisfied), we find known results that at a small enough distance upstream of the bottleneck there is the pinch region of non-interrupted synchronized flow (figure 6(*a*), (*b*)) with short enough time headways for which criterion (1) is satisfied for *none* of the time headways (figure 6(*c*), (*d*)) [12]. To explain this conclusion, we note that in accordance with [14] a moving jam exhibits the characteristic feature [*J*] of a wide moving jam (section 1), when in condition (1) $I_{\mathrm{s}} > 5$. For the model used in simulations (section 2.1), $\tau_{\mathrm{del}}^{(\mathrm{ac})} \approx 1.77$ s. Consequently, we can suggest that condition (1) is satisfied when $\tau_{\max} > 9$ s. However, all time headways in figure 6(*c*), (*d*) are shorter than 6 s.

In contrast, under condition (32), when GPs with a non-regular pinch region occur, at the same small distance upstream of the bottleneck some long-time headways appear in the pinch region of the GP for which criterion (1) is satisfied (figure 6(*g*), (*h*)). This means that there are wide moving jams that emerge almost directly upstream of the bottleneck. This is

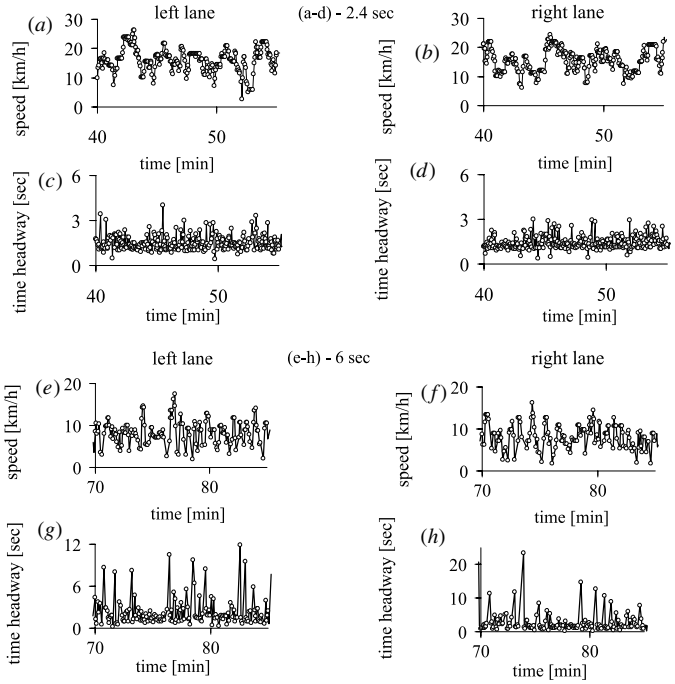

Figure 6. Simulated single-vehicle data for speed ((*a*), (*b*), (*e*), (*f*)) and time headway ((*c*), (*d*), (*g*), (*h*)) measured by a virtual detector at location 15.8 km within congested traffic in the left (figures left) and right lanes (right) related to different $T_B = 2.4$ (*a*)–(*d*) and 6 s (*e*)–(*h*). For (*a*)–(*d*) and (*e*)–(*h*) $q^{(cong)} = 1114$ and 626 vehicles/h/lane, respectively.

related to the previous result that the pinch region width $L^{(pinch)}$ of such a GP is nearly as small as zero at some random time instants (figure 5(*e*), (*g*)). During other time intervals, there is synchronized flow with short enough time headways for which criterion (1) is not satisfied (figure 6(*g*), (*h*)). Thus at small enough distances upstream of the bottleneck such GPs consist of a random alternation between synchronized flow and wide moving jams. This is related to the conclusion of section 3 that for these GPs at some random time instants the pinch region disappears and appears again.

4.2. Moving blanks within wide moving jams

Single-vehicle data measured by a virtual road detector 6 km upstream of the bottleneck within the GPs with regular (figure 7(*a*)–(*d*)) and non-regular pinch regions (figure 7(*e*)–(*h*)) exhibits qualitatively the same and typical time dependences of the speed and time headway for a sequence of wide moving jams of a GP [14]. We see that there are moving jams within which the maximum time headway τ_{max} between two vehicles within the jams is very long, i.e., traffic flow is interrupted and criterion (1) is satisfied (figure 7(*c*), (*d*), (*g*), (*h*)). Therefore, these jams are wide moving ones. There are time intervals between these jams within which the speed is high (figure 7(*a*), (*b*), (*e*), (*f*)) and vehicle time headways are small (figure 7(*c*), (*d*), (*g*), (*h*)). These regions between the wide moving jams are related to non-interrupted traffic flow. Thus at some distance upstream of the bottleneck there is a sequence of wide moving jams that is characteristic for GPs.

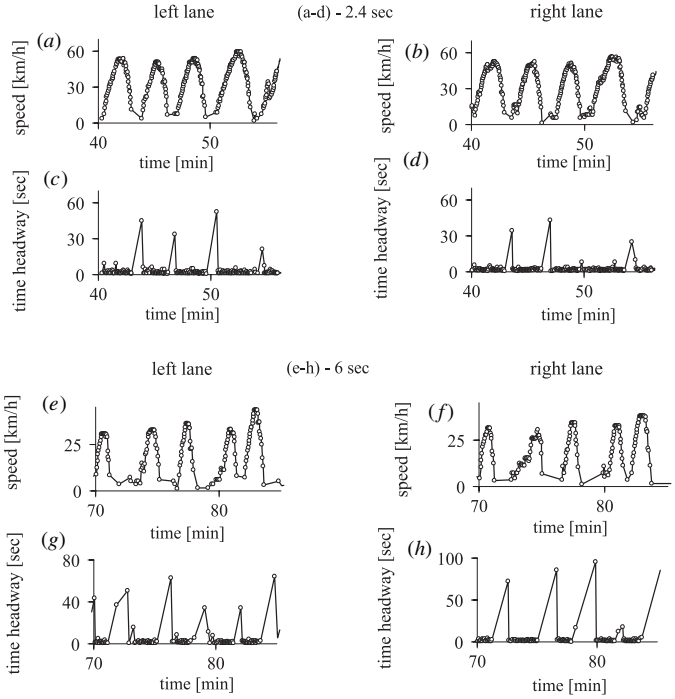

Figure 7. Simulated single-vehicle data for speed ((*a*), (*b*), (*e*), (*f*)) and time headway ((*c*), (*d*), (*g*), (*h*)) measured by a virtual detector at location 10 km within congested traffic in the left (figures left) and right lanes (right) related to different $T_{\mathrm{B}} = 2.4$ (*a*)–(*d*) and 6 s (*e*)–(*h*).

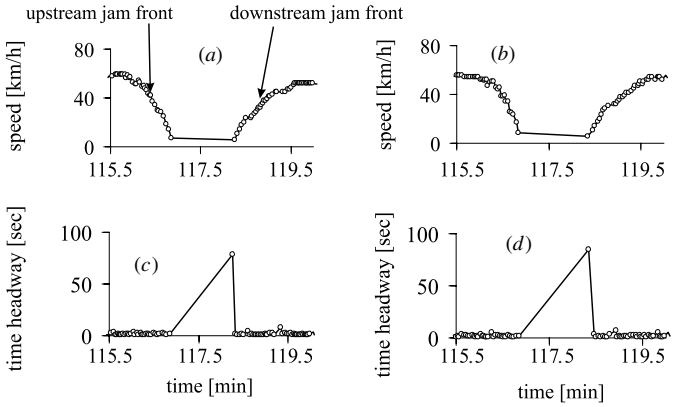

Figure 8. Simulated single-vehicle data for speed ((*a*), (*b*)) and time headway ((*c*), (*d*)) measured by a virtual detector at location 10 km within a wide moving jam in the left (figures left) and right lanes (right) related to $T_{\mathrm{B}} = 2.4$ s.

In general, a wide moving jam consists of alternations of flow interruption intervals and moving blanks within the jam. When a wide moving jam propagates upstream through a virtual detector on the road, the speed decreases sharply within the upstream jam front (figure 8(*a*), (*b*)). Then a flow interruption interval, i.e., a long-time headway that satisfies criterion (1) is usually measured (figure 8(*c*), (*d*)).

In the simplest case, the microscopic structure of a wide moving jam consists solely of this flow interruption interval only ($\tau_{\max} \approx 78.8$ and 84.8 s in the left and right lanes, respectively in figure 8(*c*), (*d*)). In this case, after the flow interruption interval the speed increases sharply within the downstream front of the jam associated with vehicles accelerating at this jam front (figure 8(*a*), (*b*)). There are no moving blanks within this jam.

In a more general case, for a wide moving jam we observe two or more flow interruption intervals, i.e., two or more long-time headways $\tau^{(i)}, i = 1, 2, \ldots$ each of them satisfies criterion (1), i.e.[4],

$$I_{\mathrm{s}}^{(i)} = \frac{\tau^{(i)}}{\tau_{\mathrm{del}}^{(\mathrm{ac})}} \gg 1, \qquad i = 1, 2, \ldots. \tag{38}$$

Between these flow interruption intervals, we find one or more vehicles that have passed the detector with speeds, which are considerably lower than the average speed both upstream and downstream of the wide moving jam. This low-speed vehicle motion is associated with moving blanks: the flow interruption intervals $\tau^{(i)}, i = 1, 2, \ldots$ are separated by one or more moving blanks within the wide moving jam.

A case, when after the first flow interruption interval only one vehicle has passed the detector location before the second flow interruption interval begins, is shown in figure 9(*a*)–(*d*). Here, only one moving blank propagates in the left lane and one moving blank propagates in the right lane, i.e., only two vehicles pass the detector during the jam propagation through the detector. The moving blanks occur at different time instants (91.28 min and 90.92 min in the left and right lanes, respectively) separating two different flow interruption intervals $\tau^{(1)} \approx 46.2$ and $\tau^{(2)} \approx 16.4$ s in the left lane and $\tau^{(1)} \approx 27.4$ and $\tau^{(2)} \approx 37.3$ s in the right lane.

In another case shown in figure 9(*e*)–(*h*), there is one moving blank only in the right lane whereas no moving blanks propagate through the detector in the left lane. There are many other cases with arbitrary variety of moving blanks in different lanes. For example, in a case shown in figure 9(*i*)–(*l*), as in the former case there are no moving blanks in the left lane, however, in the right lane there are two separated flow interruption intervals with $\tau^{(1)} \approx 46.2$ and $\tau^{(2)} \approx 19.9$ s separated by a region of four moving blanks following each other.

In all cases discussed above for GPs, respectively, with regular (figure 9(*a*)–(*d*)) and non-regular pinch regions (figure 9(*e*)–(*l*)), we can clear distinguish low-speed vehicle motions associated with moving blanks within the jams and non-interrupted flows between the jams. This is because of two features of wide moving jams: (i) the moving blanks are between flow interruption intervals satisfying criterion (38) within the jams; (ii) the speed within vehicle motion associated with moving blanks is $v \lesssim 10$ km h^{-1}, i.e., this speed is considerably lower than the average speed within flows between the jams.

4.3. Complex spatiotemporal dynamics of flow interruption intervals and moving blanks

At low scales in time and space, both GPs with a regular (figure 10(*a*), (*b*)) and non-regular pinch regions (figure 10(*c*), (*d*)) exhibit *spatiotemporal microscopic structures* in which regions of lower speed alternate with regions of higher speed; in both cases, we find that these regions propagate upstream. At the first glance, we can see only that the mean frequency of low-speed regions increases with the increase in T_{B}, i.e., when the bottleneck strength increases; this result has already been mentioned in section 3. However, if we consider the microscopic structures of GPs with a non-regular pinch region in larger scales in space and time (figures 11

[4] As mentioned above, we suggest that condition (38) is satisfied when $\tau^{(i)} > 9$ s.

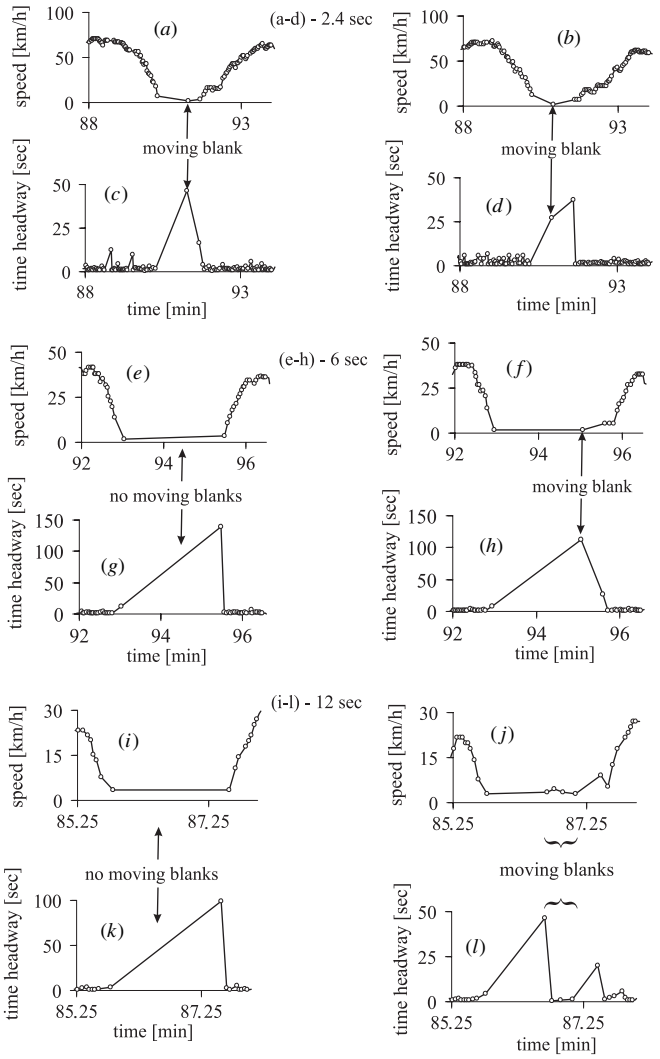

Figure 9. Simulated single-vehicle data for speed ((*a*), (*b*), (*e*), (*f*), (*i*), (*j*)) and time headway ((*c*), (*d*), (*g*), (*h*), (*k*), (*l*)) measured by a virtual detector at location 5 km within wide moving jams in the left (figures left) and right lanes (right) related to $T_{\mathrm{B}} = 2.4$ (*a*)–(*d*), 6 (*e*)–(*h*) and 12 s (*i*)–(*l*).

and 12), we can see that there is a crucial qualitative difference between them and the microscopic structures of GPs with a regular pinch region (figure 10(*a*), (*b*)).

GPs with a regular pinch region exhibits a well-known regular dynamics of wide moving jams when the jams propagate upstream of the pinch region on a homogeneous road (figure 10(*a*), (*b*)): some of the wide moving jams can dissolve during their upstream propagation (a so-called jam suppression effect) [12]. An example of the effect of the dissolution of wide moving jams can be seen in figure 10(*b*) (labeled 'jam dissolution').

However, under condition (32), i.e., when a GP with a non-regular pinch region is realized, wide moving jams of the GP can exhibit complex and non-regular spatiotemporal dynamic behavior (figures 11 and 12). This non-regular jam dynamics is associated with the following

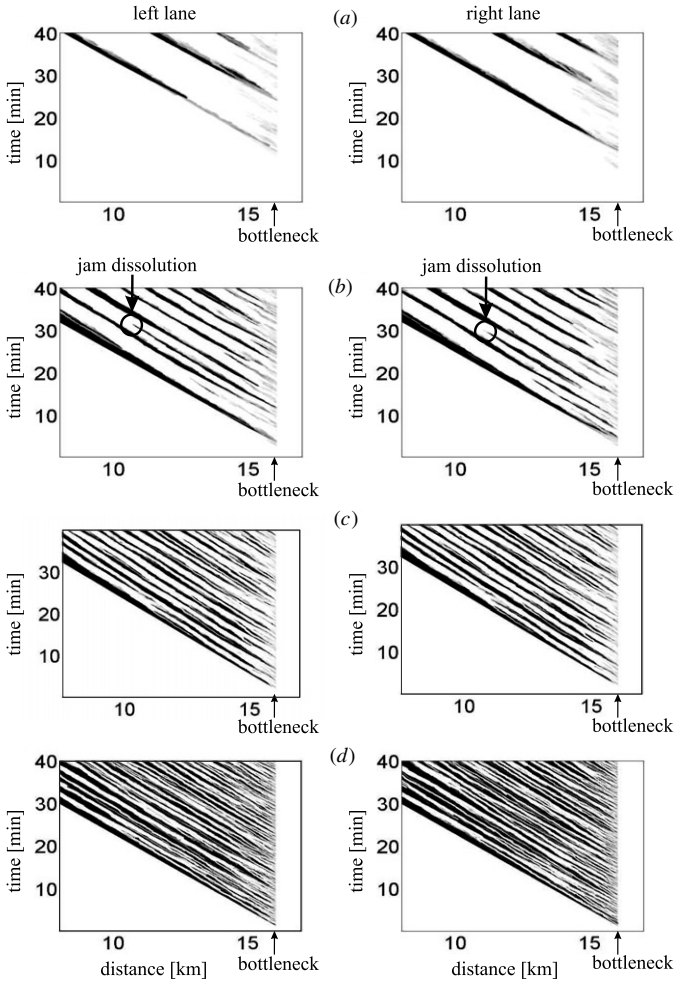

Figure 10. Simulated spatiotemporal microscopic structures of GPs with regular ((*a*), (*b*)) and non-regular pinch regions ((*c*), (*d*)): single-vehicle speeds within GPs presented in space and time by regions with variable darkness (the lower the speed, the darker the region) in the left (figures left) and right (right) road lanes associated with speed distributions at different $T_{\mathrm{B}} = 1.8$ (*a*), 2.4 (*b*), 4 (*c*), 12 s (*d*). For (*c*) $q^{(\mathrm{cong})} = 776$ vehicles/h/lane. The upstream boundary of the bottleneck region is at location $x = 16$ km (labeled 'bottleneck').

effects:

(1) The effect of the *splitting* of a flow interruption interval onto two (or more) flow interruption intervals (figures 11(*a*) and 12(*c*)).
(2) The effect of the *emergence* of a new flow interruption interval (figures 11(*a*) and 12(*d*)).
(3) The effect of the *merging* of two (or more) traffic flow interruption intervals (figures 11(*a*) and 12(*a*)).
(4) The effect of the *dissolution* of two (or more) traffic flow interruption intervals (figures 11(*b*), (*c*) and 12).

The dynamic effects (1)–(4) occur spontaneously during upstream propagation of wide moving jams. In different lanes, these effects occur often independently of each other

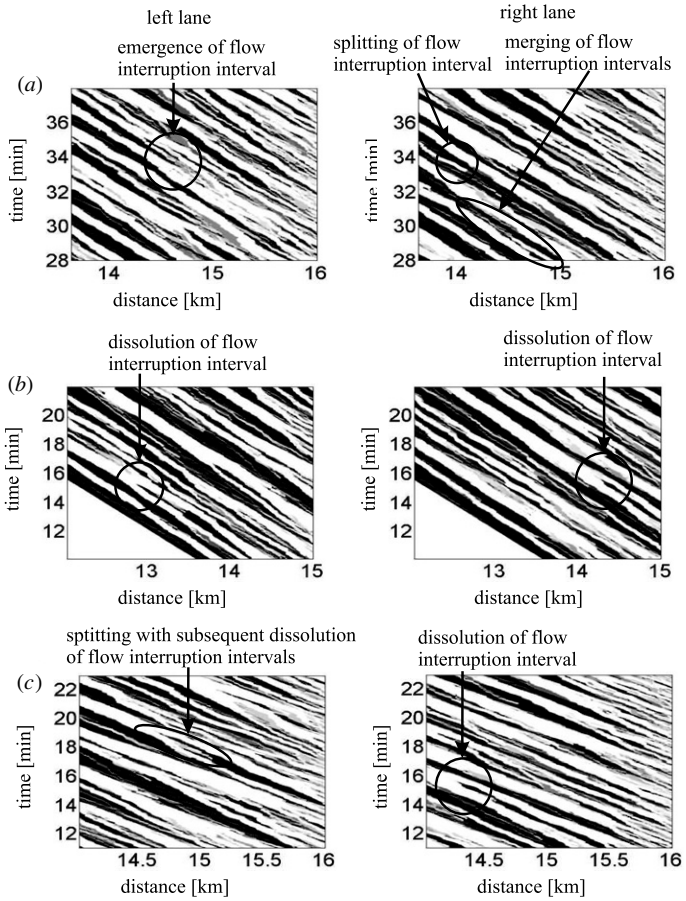

Figure 11. Fragments of figure 10(*d*) in larger scales in time and space in the left (figures left) and right lanes (right). White regions (single-vehicle speeds are equal to or higher than 5.4 km h^{-1}) are related to synchronized flows and moving blanks. Black regions (single-vehicle speeds are equal to zero) are related to flow interruption intervals. $T_B = 12$ s.

and at different road locations. A spatiotemporal competition of these effects as well as a diverse variety of the *initiating* and *resulting* dynamic effects determine a non-regular dynamic behavior of wide moving jams. The variety of the initiating and resulting effects associated with the effects (1)–(4) is as follows:

(i) The splitting of a flow interruption interval within a wide moving jam can result from the emergence of a new region of moving blanks within the jam.

(ii) The splitting of a flow interruption interval within an initial wide moving jam can result in the splitting of the jam onto two (or more) wide moving jams; in the latter case, synchronized flow(s) (or free flow(s)) occurs that separates the emergent wide moving jams. This is related to an J $\rightarrow$ S (or J $\rightarrow$ F) transition(s) occurring within the initial jam.

(iii) The effect of the emergence of a new flow interruption interval within a wide moving jam can result from the splitting of a region of moving blanks onto two (or more) regions of moving blanks separated by the emergent flow interruption interval.

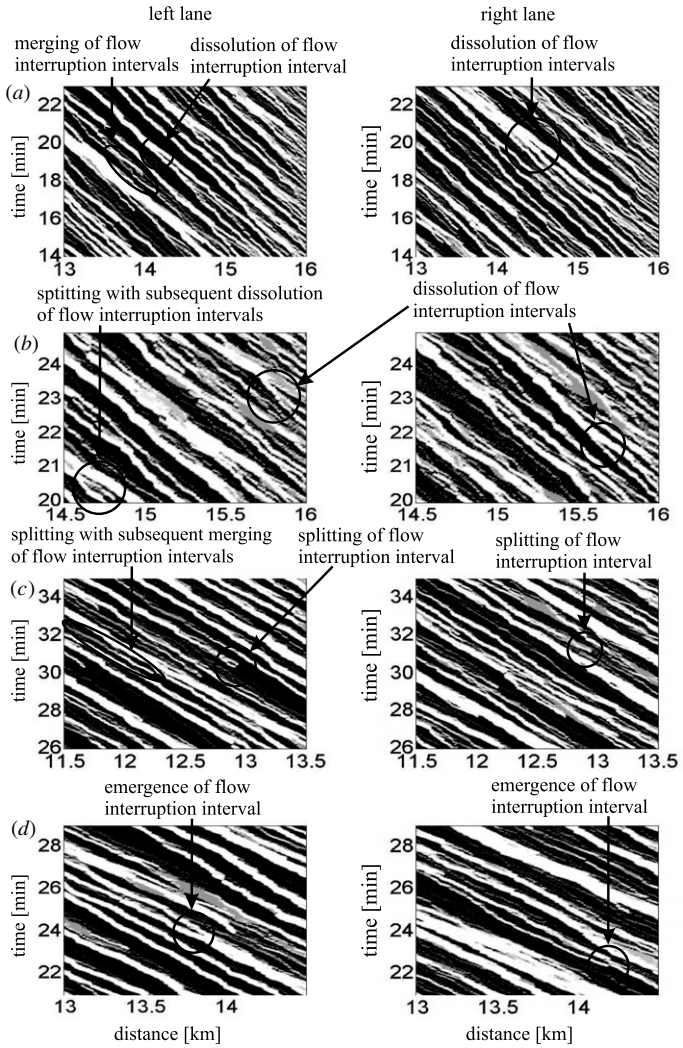

Figure 12. Simulated single-vehicle speeds within GPs presented in space and time by regions with variable darkness (the lower the speed, the darker the region) in the left (figures left) and right lanes (right). White regions (single-vehicle speeds higher than 3.6 km h^{-1}) are related to synchronized flows and moving blanks. Black regions (single-vehicle speeds are equal to zero) are related to flow interruption intervals. $T_B = 30$ s. $q^{(cong)} = 218$ vehicles/h/lane.

(iv) The effect of the emergence of a new flow interruption interval occurring within synchronized flow between two wide moving jams can result in the emergence of a new wide moving jam. This is related to an S $\rightarrow$ J transition occurring in metastable synchronized flow between the jams.

(v) The effect of the merging of two (or more) traffic flow interruption intervals can result from the dissolution of two (or more) regions of moving blanks within a wide moving jam without wide moving jam dissolution.

(vi) The effect of the merging of two (or more) traffic flow interruption intervals can result in the merging of two (or more) wide moving jams.

(vii) The effect of the dissolution of a traffic flow interruption interval within a wide moving jam can result from the merging of two (or more) regions of moving blanks within the jam.

(viii) The effect of the dissolution of a traffic flow interruption interval can result in the dissolution of a wide moving jam.

The initiating and resulting effects (v)–(viii) decrease the mean frequency of regions of flow interruption intervals and regions of moving blanks within wide moving jams as well as the mean frequency of wide moving jams of a GP. In particular, the effects (vii) and (viii) occur very frequently close to the upstream boundary of the pinch region of GPs (see road locations between 16 km and 15 km in figures 11(*a*), (*c*) and 12(*a*), (*b*)). This leads to a decrease in the mean frequency of wide moving jams, when the jams propagate upstream.

There can be diverse sequences of the effects (1)–(4) over time with a random and arbitrarily sequence of the effects (i)–(viii). For example, the splitting of a flow interruption interval onto two intervals can be followed by the subsequent dissolution of these two intervals (figures 11(*c*) and 12(*b*)); the splitting of a flow interruption interval onto two intervals can be followed by the subsequent merging of these two intervals (figure 12(*c*)). The random and arbitrarily spatiotemporal sequence of the effects discussed can explain the non-regular spatiotemporal jam dynamics found in GPs with a non-regular pinch region. In turn, this non-regular spatiotemporal jam behavior can also explain the result of section 3 that we cannot distinguish a sequence of wide moving jams in 1 min average data (figure 4(*i*)–(*l*)): the microscopic non-regular jam dynamics is averaged in this 1 min average data leading to non-regular and non-homogeneous speed distributions in which this real fine spatiotemporal jam dynamics *cannot be found*.

The complexity of the non-regular jam dynamics depends on the distance upstream of the bottleneck (figure 13). The greater this distance, the wider the mean jam width, the smaller the mean distance between wide moving jams and the smaller the mean frequencies of the effects (ii), (iv), (vi) and (viii), which are in the most degree responsible for the non-regular jam dynamics. This means that the complexity of the jam dynamics becomes the weaker, the more the distance upstream of the bottleneck. In addition, with the increase in the distance upstream of the bottleneck the mean frequency of the jams decreases. However, this decrease is limited by a limit jam frequency about 0.5 min^{-1} far enough of the bottleneck. This limit jam frequency is also related to other GPs at a great enough bottleneck strength under condition (32).

5. The microscopic spatiotemporal structure of a mega-jam

The crucial difference between GPs and a mega-jam, which occurs under condition (34), is as follows: far enough upstream of the bottleneck, single-vehicle data of a GP shows a sequence of wide moving jams separated by non-interrupted flows (figure 7); in contrast, within the mega-jam we can distinguish *no* sequence of wide moving jams (figure 14(*a*)–(*d*)). Rather than a sequence of wide moving jams, within the mega-jam there is a complex sequence of upstream moving flow interruption intervals (black regions in figure 15) for which criterion (38) is satisfied (figure 14(*c*), (*d*)). These flow interruption intervals are separated by short time intervals within which vehicles move with low speeds (figure 14(*c*), (*d*)). The latter time intervals are associated with moving blanks (white regions in figure 15).

Thus as the microscopic spatiotemporal structure of a wide moving jam, the microscopic structure of a mega-jam consists of an alternation of flow interruption intervals and moving blanks. This explain the term *mega-wide moving jam* (mega-jam) that is also a wide moving

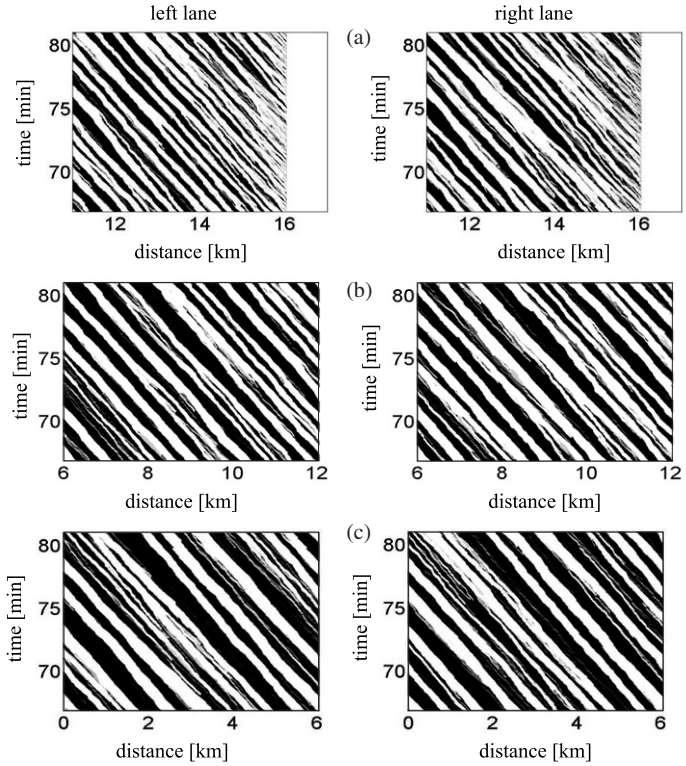

Figure 13. Simulations of dependence of non-regular jam dynamics on distance from bottleneck in the left (figures left) and right lanes (right). White regions (single-vehicle speeds higher than 5.4 km h^{-1}) are related to synchronized flows and moving blanks. Black regions (single-vehicle speeds are equal to zero) are related to flow interruption intervals. $T_B = 12$ s.

jam, however, with an extremely great width continuously growing over time. The continuous growth of the mega-jam width occurs as long as the flow rate upstream of the mega-jam q_{in} exceeds $q^{(cong)}$ (figure 2(*d*)). As for GPs with a non-regular pinch region, within the mega-jam we found a very complex and non-regular spatiotemporal dynamics of flow interruption intervals and moving blanks. Because within the mega-jam there are no wide moving jams separated by non-interrupted flows, the non-regular mega-jam dynamics is associated with the dynamic effects (i), (iii), (v) and (vii) of section 4.3 only. When the bottleneck strength increases further, the microscopic spatiotemporal structure of traffic congestion does not qualitatively change any more (figure 16). However, time intervals within which moving blanks occur become shorter.

As the complexity of the non-regular jam dynamics (section 4.3), the complexity of the non-regular mega-jam dynamics depends also on the distance upstream of the bottleneck (figures 15 and 16). The greater this distance, the wider the mean width of flow interruption intervals and the smaller the mean frequencies of the dynamic effects (i), (iii), (v) and (vii) that are responsible for the non-regular mega-jam dynamics. This means that the complexity of the mega-jam dynamics becomes the weaker, the more the distance upstream of the bottleneck.

At a small distance upstream of the bottleneck, single-vehicle data for a GP for which the pinch region dissolves fully (figure 17(*a*)–(*d*)) and for a mega-jam (figure 17(*e*)–(*h*)) exhibit

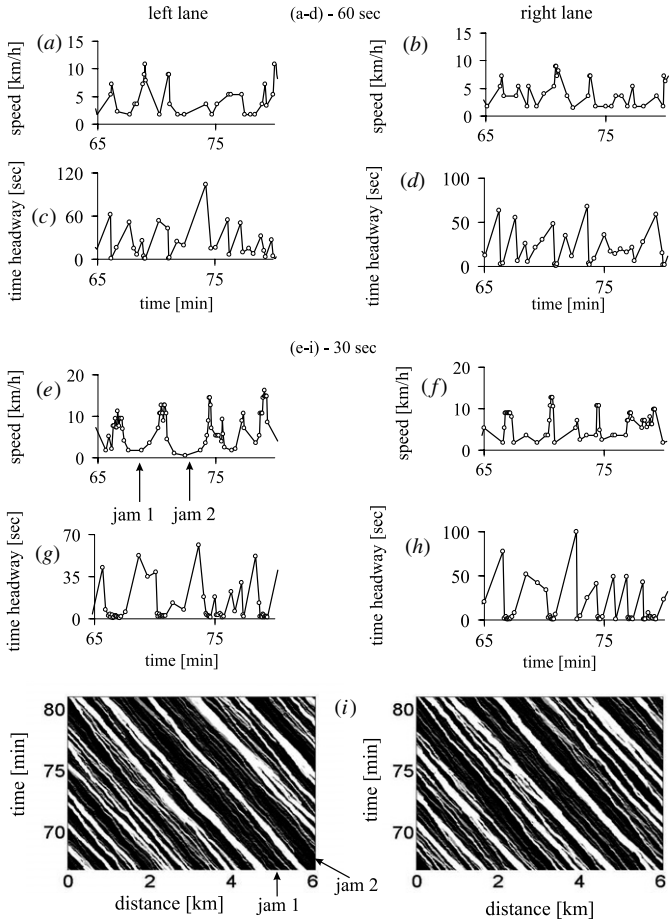

Figure 14. Simulated single-vehicle data for speed ((*a*), (*b*), (*e*), (*f*)) and time headway ((*c*), (*d*), (*g*), (*h*)) measured by a virtual detector at location $x = 5$ km related to $T_B = 60$ (*a*)–(*d*) and 30 s (*e*)–(*h*), as well as single-vehicle speed data within GP for $T_B = 30$ s presented in space and time by regions with variable darkness (the lower the speed, the darker the region). In (i), white regions (single-vehicle speeds higher than 3.6 km h^{-1}) are related to synchronized flows and moving blanks and black regions (single-vehicle speeds are equal to zero) are related to flow interruption intervals. Left and right figures are related to the left and right lanes, respectively. The upstream boundary of the bottleneck is at location $x = 16$ km.

qualitatively the same features: in both cases congested traffic consists of an alternation of flow interruption intervals, for which condition (38) is satisfied, and moving blanks.

It should be noted that in contrast with GPs related to $T_B \leqslant 12$ s (figures 7 and 9), the difference between a GP for which the pinch region dissolves fully, which is associated with conditions $T_B^{(th)} \leqslant T_B < T_B^{(mega)}$ that results in

$$q_{th}^{(cong)} \geqslant q^{(cong)} > q_{mega}^{(cong)}, \tag{39}$$

and a mega-jam associated with condition (34) cannot also be clearly seen upstream of the bottleneck: it is not easy to distinguish wide moving jams separated by non-interrupted flows for this GP (figure 14(*e*)–(*i*)). This is because under condition (39) for the model

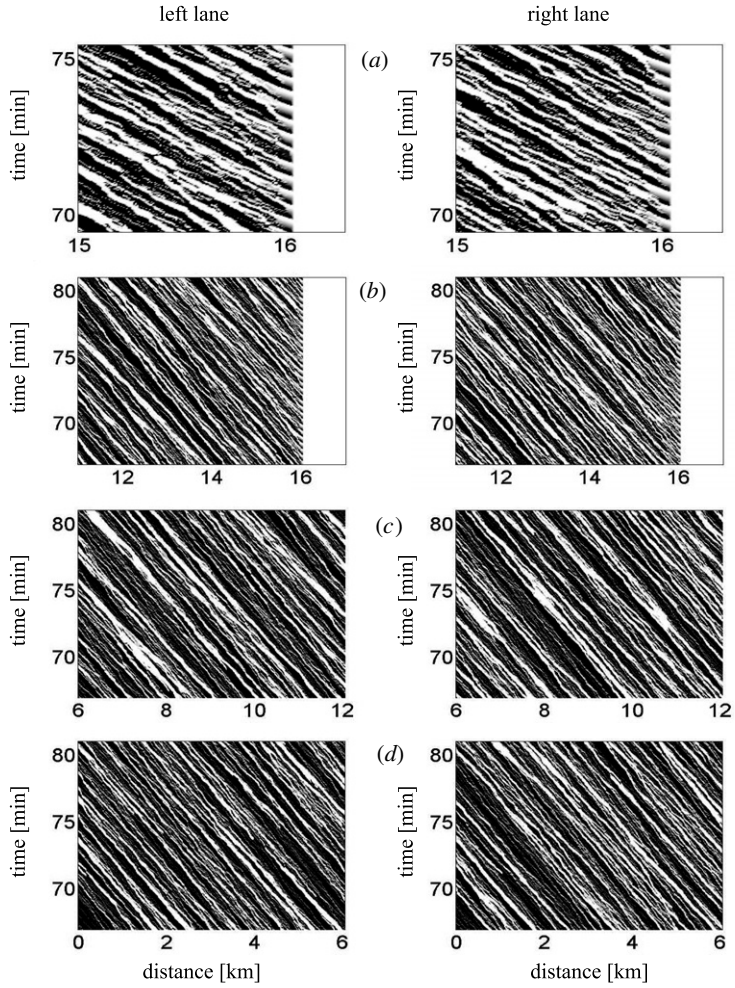

Figure 15. Fragments of figure 10(*d*) in larger scales in the left (figures left) and right lanes (right). White regions (single-vehicle speeds higher than 1.8 km h^{-1}) are related to moving blanks. Black regions (single-vehicle speeds are equal to zero) are related to flow interruption intervals. $T_B = 60$ s. The upstream boundary of the bottleneck is at location $x = 16$ km.

of identical vehicles used in simulations (section 2.1) the difference between the flow rates $q^{(\text{blanks})}$ and $q^{(\text{cong})}$ is very small. For example, for the GP at $T_B = 30$ s, the flow rate $q^{(\text{cong})} = 218$ vehicles/h/lane, whereas $q^{(\text{blanks})} \approx 130$ vehicles/h/lane. In addition, for this GP the average speed between wide moving jams that is about 15 km h^{-1} (figure 14(*e*), (*f*)) is not considerably higher than the speed associated with moving blanks. For these reasons, we can distinguish only a few separated wide moving jams within this GP far enough upstream of the bottleneck (for example, the jams labeled 'jam 1' and 'jam 2' in figure 14(*e*)–(*i*) can be considered as separated ones because flow rates between the jams are greater than 800 vehicles/h/lane, i.e., they exceed $q^{(\text{blanks})}$ considerably). Thus under condition (39) GPs exhibit intermediate features between the features of mega-jams and the features of GPs with non-regular sequences of wide moving jams found in section 4.3.

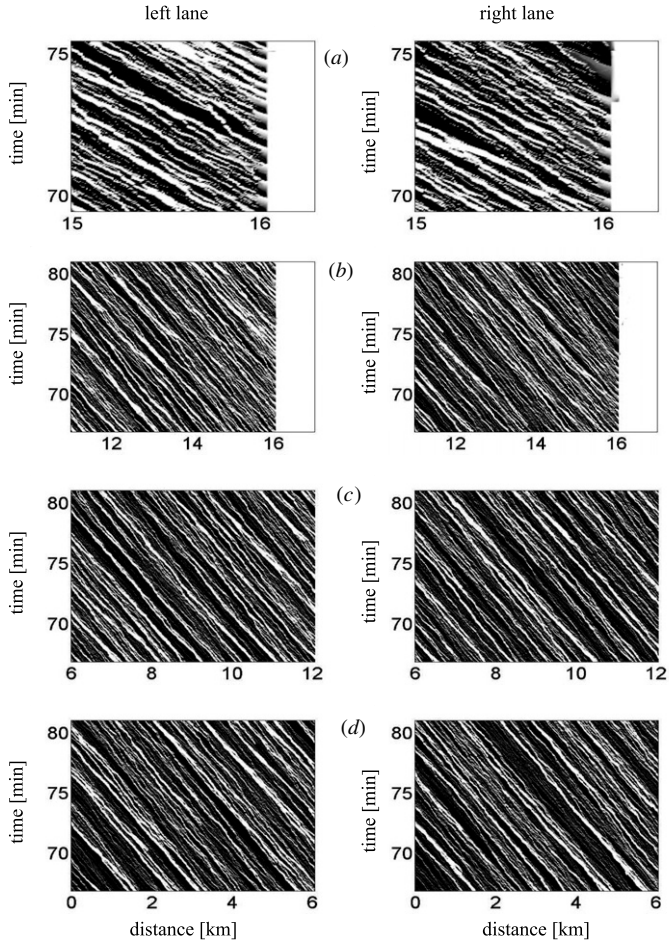

Figure 16. Simulated single-vehicle speed data within mega-jam presented in space and time by regions with variable darkness (the lower the speed, the darker the region). White regions (single-vehicle speeds higher than 1.8 km h^{-1}) are related to moving blanks and black regions (single-vehicle speeds are equal to zero) are related to flow interruption intervals. Left and right figures are related to the left and right lanes, respectively. $T_B = 90$ s. $q^{(cong)} = 95$ vehicles/h/lane. The upstream boundary of the bottleneck is at location $x = 16$ km.

6. Discussion

6.1. Random jam nucleation in metastable synchronized flow resulting in non-regular spatiotemporal dynamics of moving jams

For explanations of the results of the paper, we should recall some features of an S $\rightarrow$ J transition, which is a first-order phase transition (figure 18) [12, 35]. We consider a wide moving jam consisting of a flow interruption interval only; we suggest that the vehicle density within the jam $\rho_{max} = 1/d$, where d is the vehicle length (section 2.1). Flow states directly *downstream* the jam are related on average to the line J whose slope is equal to the mean velocity v_g of the downstream front of the jam. If a flow state directly *upstream* of the jam is associated with a point in the flow-density plane that is *below* the line J (point labeled

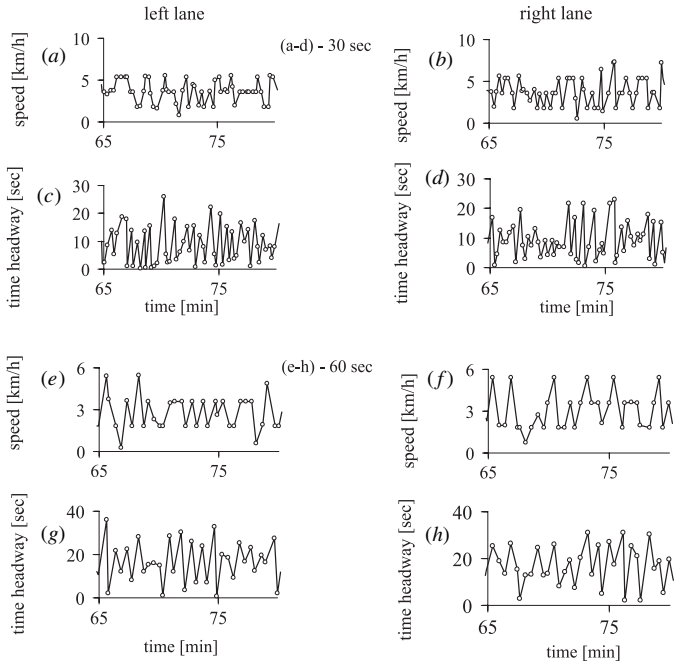

Figure 17. Simulated single-vehicle data for speed ((*a*), (*b*), (*e*), (*f*)) and time headway ((*c*), (*d*), (*g*), (*h*)) measured by a virtual detector at location $x = 15.8$ km, i.e., 200 m upstream of the upstream boundary of the bottleneck in the left (figures left) and right lanes (right) related to $T_B = 30$ (*a*)–(*d*) and 60 s (*e*)–(*h*).

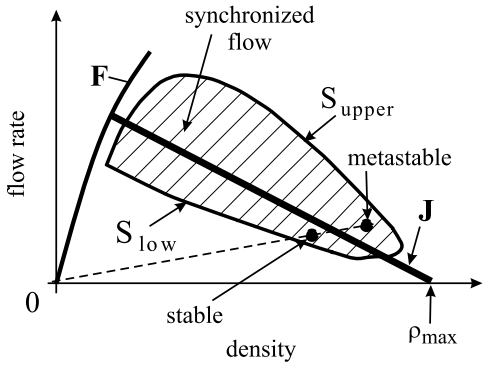

Figure 18. Qualitative explanation of features of moving jam emergence [35]: free flow (*F*), steady states of synchronized flow (2D dashed region) and the line *J* in the flow density plane. A dashed line is related to a given low synchronized flow speed.

'stable' in figure 18), then the absolute value of the velocity of the upstream front of this jam $\left|v_g^{(up)}\right| < |v_g|$ (the velocity $\left|v_g^{(up)}\right|$ is associated with the slope of a line in the flow-density plane from the point 'stable' to the point $(0, \rho_{max})$ related to the jam). This means that the jam width, i.e., the duration of the flow interruption interval decreases over time. In contrast, if a flow state directly upstream of the jam is associated with a point in the flow-density plane

that is *above* the line J (point labeled 'metastable' in figure 18), then the absolute value of the velocity of the upstream front of this jam $\left|v_g^{(up)}\right| > |v_g|$, i.e., the jam width, i.e., the duration of the flow interruption interval increases over time. This can explain why all synchronized flow states below the line J are stable, whereas all synchronized flow states on and above the line J are metastable with respect to wide moving jam emergence (S $\rightarrow$ J transition) [35].

As shown in [12, 16], the random moving jam emergence in metastable synchronized flow, which is qualitatively discussed above, is simulated in the stochastic traffic flow model through a competition between the speed adaptation and over-deceleration effects (items (iii) and (vi) of section 2.1). In particular, simulations show that in metastable synchronized flow (states on and above the line J in figures 1(*b*) and 18), a wide moving jam emerges spontaneously, if a speed disturbance occurs within which the speed is equal to or lower than a critical speed required for an S $\rightarrow$ J transition; otherwise the disturbance decays and no an S $\rightarrow$ J transition occurs (see related simulation results in section 6.5). Thus a speed disturbance with the critical speed can be considered a nucleus for an S $\rightarrow$ J transition; the nucleus for an S $\rightarrow$ J transition that subsequently grows propagating upstream has been called a growing narrow moving jam. At a given distant of different synchronized flow points associated with various speeds from the line J in the flow-density plane, the smaller the speed, the smaller the nucleus required for an S $\rightarrow$ J transition.

As usual for first-order phase transitions, simulations show also that an S $\rightarrow$ J transition is characterized by a random time delay T_{SJ} [16, 29]. T_{SJ} includes a random time delay of spontaneous nucleation of a narrow moving jam and a random time of the jam growth within the pinch region until the jam transforms into a wide moving jam at the upstream boundary of the pinch region. Thus the smaller T_{SJ}, the shorter $L^{(pinch)}$. The random character of T_{SJ} explains a time dependence of $L^{(pinch)}(t)$ (figure 5(*c*), (*e*), (*g*)). We found that the greater the bottleneck strength, i.e., the smaller the average flow rate $q^{(cong)}$ in congested traffic, the lower the speed and the greater the density within the pinch region. However, as mentioned above, the lower the speed and the greater the density in synchronized flow, the smaller the nucleus required for the emergence of a flow interruption interval, i.e., the smaller the mean random time delay $T_{SJ}^{(mean)}$.

Thus the smaller the flow rate $q^{(cong)}$, the greater the probability for the occurrence of a negligibly small T_{SJ}, i.e., the greater the probability for the emergence of wide moving jams directly upstream of the bottleneck; in the latter case $L^{(pinch)} = 0$. This explains why under condition (32) the regular structure of the GP breaks due to the random disappearance of the pinch region during some time intervals. This explains also why $L_{mean}^{(pinch)}$ decreases up to zero, when a strong decrease in $q^{(cong)}$ causes a decrease in $T_{SJ}^{(mean)}$ up to zero, i.e., when under condition (33) the pinch region does not exist.

The above physics of wide moving jam (flow interruption interval) emergence in synchronized flow incorporated in the model of section 2.1 explains also complex dynamics of wide moving jams found under condition (32). Upstream of the pinch region, synchronized flows between flow interruption intervals are related on average to points on the line J in the flow-density plane. However, there are random disturbances in these flows; some of them decrease the speed and increase the density (i.e., time headways decrease), other disturbances decrease the density (i.e., time headways increase). As explained above, a speed disturbance, which decreases the speed, can lead to the emergence of a flow interruption interval, i.e., the jam emergence, when the speed becomes lower than the critical one (this case is associated with points above the line J in figure 18). In contrast, a disturbance, which decreases the density, can lead to flow interruption dissolution, when an initial flow interruption interval is short enough (this case is associated with points below the line J in figure 18). As mentioned

above, the smaller the synchronized flow speed between the jams, the smaller the nucleus required for the emergence of a flow interruption interval in this flow. At smaller bottleneck strengths, the average speed in synchronized flow between flow interruption intervals is high and the density is relatively small, and therefore, the probability of the emergence of flow interruption intervals is small.

In contrast, at greater bottleneck strengths, i.e., at smaller flow rates $q^{(\mathrm{cong})}$, the synchronized flow speed between wide moving jams is low (compare synchronized flow speeds between the jams in figures 7 and 9 for $T_{\mathrm{B}} = 2.4$, 6 and 12 s) and the density is great; therefore, the probability of the emergence of flow interruption intervals between the jams, i.e., the emergence of new wide moving jams, increases rapidly with the bottleneck strength. As a result, many short flow interruption intervals appear at smaller flow rates $q^{(\mathrm{cong})}$; in turn, other random disturbances, which cause a density decrease upstream of these emergent flow interruption intervals, lead with a great probability to the dissolution of the flow interruption intervals. A spatiotemporal competition between the random emergence and dissolution of flow interruption intervals can explain the non-regular spatiotemporal jam dynamics of section 4.3.

There are several sources for random speed disturbances in the model of section 2.1, whose growth leads to the emergence of flow interruption intervals in synchronized flows: lane changing, the variety of the random delays in vehicle acceleration and decelerations. In addition, within the bottleneck vehicles are forced to move at much longer safe time headways $\tau^{(\mathrm{safe})} = T_{\mathrm{B}}$ than away of the bottleneck $\tau^{(\mathrm{safe})} = 1$ s (section 2.2). For this reason, the mean amplitude of speed disturbances in the pinch region is considerably greater than that in synchronized flows between the jams on a homogeneous road. This explains why the non-regular jam dynamics is considerably visible only at greater bottleneck strengths than the critical bottleneck strength for the occurrence of GPs with a non-regular pinch region.

The above physics of the non-regular jam dynamics found in simulations of the stochastic traffic flow model of section 2.1 can also explain why at a given bottleneck strength the complexity of this jam dynamics becomes the weaker, the more the distance upstream of the bottleneck (figure 13): far enough upstream of the bottleneck, durations of the flows between wide moving jams become short and therefore the probability for speed fluctuations, which are great enough for the emergence of flow interruption intervals within these flows, decreases.

6.2. Physics of mega-jam

When the bottleneck strength increases strongly and condition (6), i.e., (34) is satisfied, as explained in the introduction and found in numerical simulations (section 5), wide moving jams merge into a mega-jam. The whole flow rate within any mega-jam is supplied by moving blanks *only*. As a result, under condition (6) we get

$$q^{(\mathrm{cong})} = q^{(\mathrm{blanks})}_{\mathrm{mega}}, \tag{40}$$

where $q^{(\mathrm{blanks})}_{\mathrm{mega}}$ denotes the average flow rate associated with moving blanks within the mega-jam, which satisfies the condition

$$q^{(\mathrm{blanks})}_{\mathrm{mega}} \leqslant q^{(\mathrm{blanks})}, \tag{41}$$

where $q^{(\mathrm{blanks})}$ is defined via formula (4), i.e., this is the average flow rate associated with moving blanks within wide moving jams separated by non-interrupted flows. The equality in (41) is related to (5). Thus if under condition (6) the bottleneck strength increases and therefore $q^{(\mathrm{cong})}$ decreases, then in accordance with (40), the flow rate $q^{(\mathrm{blanks})}_{\mathrm{mega}}$ decreases. This explains shorter regions of moving blanks in figure 16 in comparison with those in figure 15.

As mentioned in section 3 (see (36)), the threshold bottleneck strength for the pinch region existence is smaller than the critical bottleneck strength for the mega-jam formation. To explain that this result has a general character, let us assume that the bottleneck strength is initially greater than the critical one for the mega-jam formation. In this case, $q^{(\mathrm{cong})} = q^{(\mathrm{blanks})}_{\mathrm{mega}} < q^{(\mathrm{blanks})}$. If now the bottleneck strength decreases gradually, then the flow rate $q^{(\mathrm{cong})}$ increases. The flow rate $q^{(\mathrm{cong})}$ can be supplied by moving blanks only up to the critical bottleneck strength satisfying condition (5), i.e., $q^{(\mathrm{cong})} = q^{(\mathrm{blanks})}$. When the bottleneck strength decreases further and becomes smaller than the critical one for the mega-jam formation, then $q^{(\mathrm{cong})} > q^{(\mathrm{blanks})}$. The difference $\Delta q_{\mathrm{blanks}} = q^{(\mathrm{cong})} - q^{(\mathrm{blanks})}$ should be supplied by vehicles accelerating from wide moving jams; this means that wide moving jams separated by synchronized flows must appear in congested traffic. In particular, such synchronized flows appear just upstream of the bottleneck as a result of the upstream propagation of wide moving jams that emerge directly upstream of the bottleneck. Nevertheless, a pinch region of the synchronized flow at the bottleneck does not still appear as long as the difference $\Delta q_{\mathrm{blanks}}$ is small enough. Indeed, the pinch region appears only, when at least one of the wide moving jams occurs at a *finite distance* upstream of the bottleneck in the synchronized flow due to a growing narrow moving jam that emerges initially in this flow. This is possible only, if the former wide moving jam due to its upstream propagation is at a great enough distance from the bottleneck. The latter can be realized, when the difference $\Delta q_{\mathrm{blanks}}$ exceeds also some *finite value*, i.e., the threshold bottleneck strength for the pinch region existence should be always smaller than the critical one for the mega-jam formation. Thus condition (36) is a general result for any heavy bottleneck.

Simulations allow us to assume that moving blanks can be considered speed fluctuations within the wide moving jam phase. Consequently, the non-regular dynamics effects (i), (iii), (v) and (vii) of section 4.3 can be explained by great amplitude of speed fluctuations associated with moving blanks occurring during their upstream propagation. This assumption is confirmed by empirical observations of very broad distributions of vehicles time headways associated with moving blanks [14]. Moreover, a random time delay in vehicle acceleration from a vehicle standstill within a flow interruption interval can cause fluctuations in the velocity of the downstream front of the flow interruption interval.

6.3. Comparison with empirical results

To compare the above theory of traffic congestion with empirical congested patterns, one should have measured data for traffic congestion at a bottleneck, whose strength should be manually continuously changeable from the one associated with usual bottlenecks like on- and off-ramps to great bottleneck strengths associated with heavy bottlenecks caused, e.g., by bad weather conditions or accidents, specifically when condition (2) is not valid. Unfortunately, such measured data are not available. However, we can compare the theory with 1 min average data measured at several road locations within congested patterns related to two limiting cases: (i) traffic congestion at a usual on-ramp bottleneck and (ii) traffic congestion at a heavy bottleneck.

Speed distributions within congested patterns found in simulations (figures 2(*a*), (*b*) and 19) for the range of $T_{\mathrm{B}} = 1.6 - 2.4$ s associated with the flow rate range

$$q^{(\mathrm{cong})} = q^{(\mathrm{pinch})} = 1113\text{–}1800 \text{ vehicles/h/lane} \tag{42}$$

are qualitatively the same as those in an empirical GP shown in figure 20(*a*), (*b*) and in all other known empirical GPs [12]. Moreover, quantitative values of empirical flow rates $q^{(\mathrm{pinch})}$ (2) are approximately associated with the theoretical result (42). Empirical speed autocorrelation

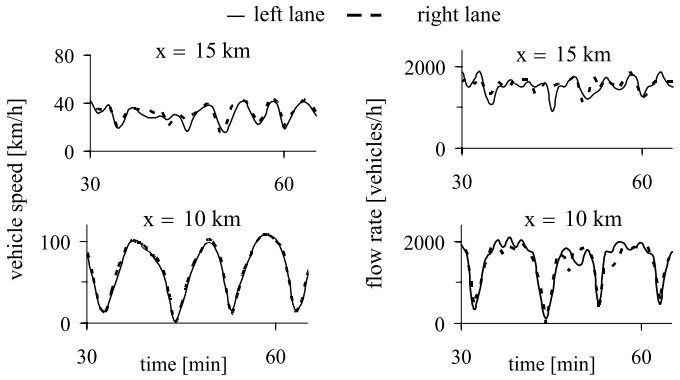

Figure 19. Simulation results for speed (left) and flow rate (right) associated with locations within the pinch region ($x = 15$ km) and the sequence of wide moving jams ($x = 10$ km) of the GP shown in figure 2(*a*). The upstream boundary of the bottleneck is at $x = 16$ km. 1 min average data.

functions and associated Fourier spectra of speed time dependencies show regular character of wide moving jam propagation (figure 20(*c*), (*d*)) as those found in simulations of GP at shorter T_B (figure 4(*c*), (*d*)).

In contrast, for $T_B > 6$ s associated with the average flow rate $q^{(\text{cong})} < 625$ vehicles/h/lane simulated congested patterns at heavy bottlenecks (figure 2(*c*), (*d*)) are qualitatively the same as those we found in empirical data measured on many various days (and years) on different freeways, when very heavy bottlenecks caused by bad weather conditions or accidents occur for which empirical flow rates

$$q^{(\text{cong})} \lesssim 600 \text{ vehicles/h/lane}. \tag{43}$$

In this case, rather than regular structure of traffic congestion of GPs (figures 2(*a*), (*b*), 19, and 20), both theoretical (figures 2(*c*), (*d*), 4(*i*) and 21) and empirical traffic congested patterns (figure 22) exhibit non-regular spatiotemporal structure of congestion in which *no* sequences of wide moving jams can be distinguished in 1 min average data.

An example of such an empirical congested traffic pattern is shown in figure 22. Rather than the regular structure of congestion within the GP (figure 20), in measured data associated with bad weather conditions a non-regular spatiotemporal structure of congestion is observed (figure 22). A heavy bottleneck appears on February 02, 2006 between locations 4.07 and 3.02 km due to snow and ice. Upstream of the bottleneck, very low speed and flow rate patterns ($x \leqslant 3.02$ km in figure 22(*b*)) are observed. Downstream of the bottleneck ($x = 4.07$ km) vehicles have escaped from the congestion (speed is high); however, the flow rate is very small because the bottleneck reduced the average flow rate within the congestion strongly. For example, at $x = 3.02$ km, the flow rate $q^{(\text{cong})}$ averaged between 7:00 and 7:40 and across the road is 513 vehicles/h/lane. In contrast with the GP in figure 20(*b*) (as with other empirical GPs [12]), within traffic congestion shown in figure 22 non-regular low-speed patterns are observed in which *no* sequence of wide moving jams can be distinguished ($x \leqslant 3.02$ km). This conclusion is regardless of the flow rates to on- and off-ramps, which in the data set lead to an increase in $q^{(\text{cong})}$ at $x = 1.77$ km in comparison with $q^{(\text{cong})}$ at $x = 0$ km (figure 22(*a*), (*b*)). If speeds in different lanes are compared (figure 22(*c*)), we find even more non-regular speed time dependencies: whereas no vehicles pass a detector in one of the lanes, i.e., the speed is zero, during the same time interval the average speed in other lanes can be

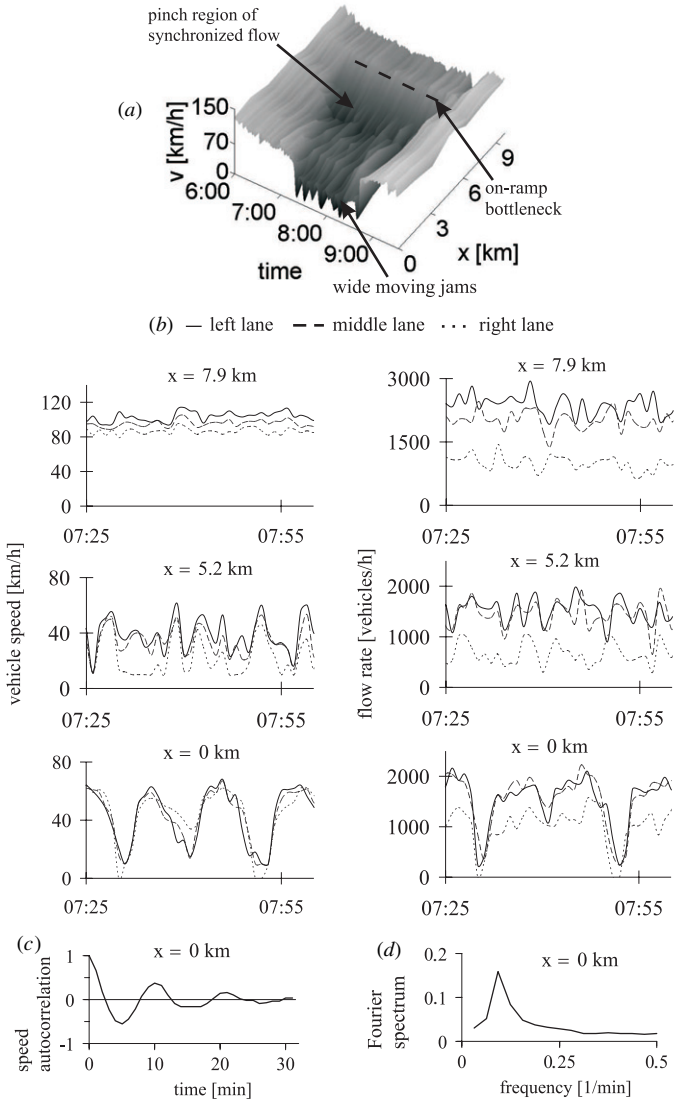

Figure 20. Usual empirical traffic congestion—a general pattern (GP) at on-ramp bottleneck. (*a*) Measured speed in space and time for the GP. (*b*) Measured speed (left) and flow rate (right) associated with (*a*) in different lanes at different road locations associated with free flow downstream of the bottleneck ($x = 7.9$ km), pinch region of synchronized flow upstream of the bottleneck ($x = 5.2$ km), and within a sequence of wide moving jams at $x = 0$ km. ((*c*), (*d*)) Empirical speed correlations (*c*) and associated Fourier spectra (*d*) for speed in the left lane within the sequence of wide moving jams at $x = 0$ km. $q^{(\text{pinch})} \approx 1200$ vehicles/h/lane. 1 min average data measured on the freeway A5-South in Germany on April 15, 1996. Arrangement of detectors is shown in figure 2.1 of the book [12].

higher than zero. This explains why in time dependences of speeds averaged across the road (figure 22(*b*)), this very low speed is seldom equal to exactly zero.

As congested traffic in measured data (figure 22(*b*), (*c*)), simulated congested traffic at a heavy bottleneck is also non-homogeneous in space and time (figures 4(*i*), (*j*) and 21).

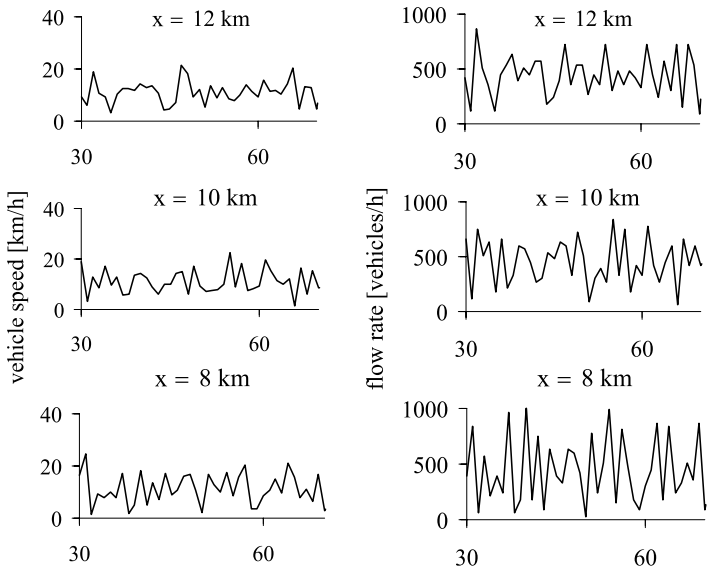

Figure 21. Simulation results for speed (left) and flow rate (right) averaged across the road at different road locations within the congested pattern shown in figure 2(*c*). The upstream boundary of the bottleneck is at $x = 16$ km. $T_B = 12$ s. 1 min average data.

In the measured and simulated data, as follows from Fourier spectra of speed time dependencies, these non-homogeneous congested patterns exhibit non-regular spatiotemporal behavior (figures 22(*d*) and 4(*l*)). This is in contrast with the regular structure of traffic congestion within the GP (figures 20 and 19).

As in measured data (figure 22(*b*), (*c*)), in 1 min average data related to traffic congestion in simulations very low speed and flow rate patterns are realized upstream of the bottleneck in which *no* sequence of wide moving jams can be distinguished (figure 21); downstream of the bottleneck ($x > 16.3$ km) vehicles have escaped from the congestion (speed is high) (figure 2(*c*)), however, the flow rate is very small because the bottleneck reduced the average flow rate within the congestion strongly.

A summary of the above comparison of theory of traffic congestion with the measured data is as follows:

(i) Spatiotemporal distributions of the 1 min average speed and flow rate within GPs occurring at usual bottlenecks are qualitatively the same in the above theory (figure 19) and measured data (figure 20(*a*), (*b*)): in both simulated and measured data, GPs consist of the pinch region and wide moving jams upstream. Measured and simulated speed autocorrelation functions and associated Fourier spectra of speed time dependencies show *regular* character of wide moving jam propagation (figures 4(*c*), (*d*) and 20(*c*), (*d*)).

(ii) In contrast with item (i), in 1 min average data related to simulated congested patterns (figure 21) and to measured data (figure 22(*b*), (*c*)) for traffic congestion at heavy bottlenecks *no* sequence of wide moving jams can be distinguished. In simulations (figure 21) and measured data (figure 22(*b*), (*c*)), spatiotemporal distributions of the average speed and flow rate in these congested patterns are non-homogeneous in space and time. Fourier spectra of the associated non-homogeneous time dependencies of the speed show non-regular character of traffic congestion at the heavy bottlenecks both in simulations (figure 4(*l*)) and measured data (figure 22(*d*)).

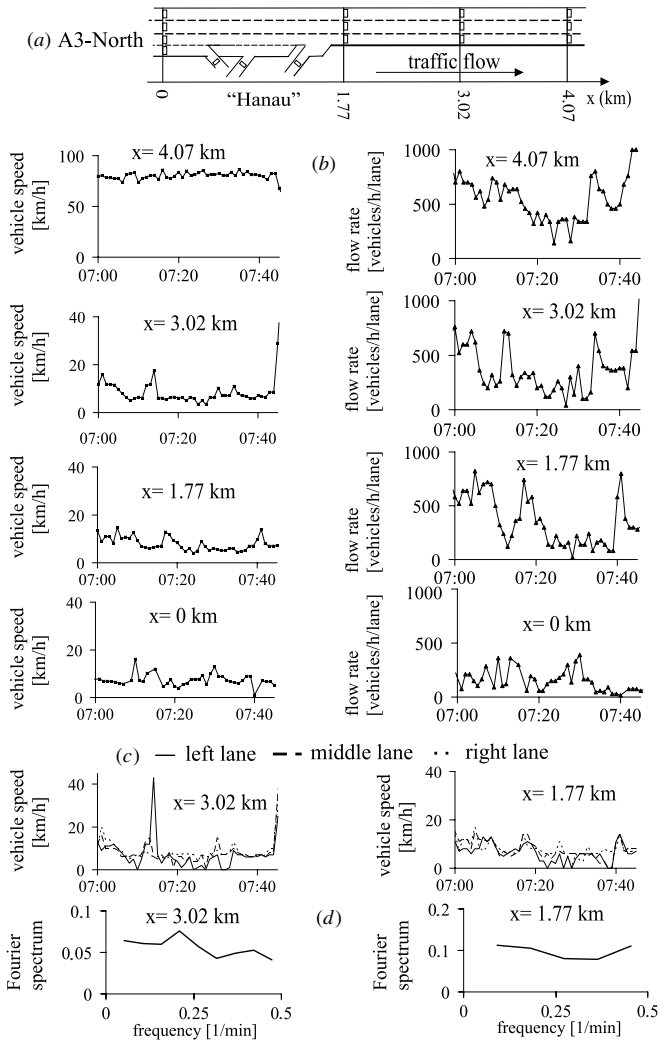

Figure 22. Empirical structure of congestion caused by snow and ice. (*a*) Scheme of road detector arrangement on a section of the freeway A3-North in Germany near the intersection 'Hanau'. (*b*) Average speed and flow rate across the freeway at different locations. (*c*) Speed in different lanes at two locations. (*d*) Fourier spectra of time dependences of the speed in the left lane at two locations. 1 min average data.

As follows from sections 4.3 and 5, the non-regular pattern behavior of item (ii) can be explained by two different reasons:

(1) The occurrence of a GP with the non-regular dynamics of wide moving jams.
(2) The occurrence of a mega-jam.

However, based on 1 min average data these two reasons of non-regular traffic congestion cannot be distinguished from each other. Indeed, theoretical results of sections 4.3 and 5 allow us to suggest that at a very heavy bottleneck caused for example by bad weather conditions or accidents there should be a very fine microscopic spatiotemporal structure of traffic congestion associated with non-regular spatiotemporal dynamics of wide moving jams or/and flow interruption intervals as well as moving blanks. However, this theoretical structure

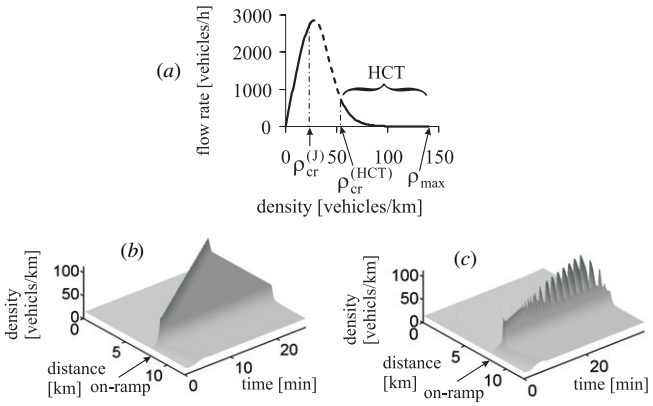

Figure 23. Example of fundamental diagram of some traffic flow models (*a*) and simulations of HCT (*a*) and OCT (*b*) at on-ramp bottleneck [7, 37, 41, 43].

of traffic congestion, even if it exists in real traffic, would be averaged in 1 min average measured data, i.e., they could not be found in these data. Thus to make a more detailed comparison of the presented theory with measured data, single-vehicle data measured within traffic congestion at heavy bottlenecks is required. Unfortunately, currently these measured single-vehicle data are not available. Such a comparison of the theory presented in the paper with measured single-vehicle data is a separate and important task of further investigations (see also section 6.5).

6.4. Critical discussion of homogeneous congested traffic

In some traffic flow models associated with the fundamental diagram approach to traffic flow modeling, for example, Payne-like macroscopic models (e.g., [36, 37]), the Aw-Rascle macroscopic model [38], optimal velocity (OV) models (e.g., [39, 40]), the intelligent driving model (IDM) [7, 43] as well as some other traffic flow models (see references in [7]), the density region at the fundamental diagram, within which traffic flow is unstable, is limited at greater densities, i.e., flow states at the fundamental diagram are unstable *only* within the density range (dashed part of the fundamental diagram in figure 23(*a*)),

$$\rho_{cr}^{(J)} < \rho < \rho_{cr}^{(HCT)}. \tag{44}$$

In other words, within the density range

$$\rho_{cr}^{(HCT)} < \rho \leqslant \rho_{max} \tag{45}$$

homogeneous model states of congested traffic related to very small flow rates $q^{(cong)}$ are stable with respect to small amplitude fluctuations. These model states, in which the speed and flow rate are *homogeneous in space and time-independent*, have been called in [7, 41] as *homogeneous congested traffic* (HCT) (figure 23(*b*)). In these traffic flow models [7, 37, 38, 40, 43], HCT can appear spontaneously upstream of a very heavy bottleneck, i.e., when the bottleneck strength is great enough. The more the bottleneck strength, the more the density exceeds $\rho_{cr}^{(HCT)}$ and the more stable is HCT with respect to non-homogeneous speed disturbances in these models [7, 37, 38, 40, 43][5].

[5] It must be noted that HCT is not a general result of traffic flow models in the framework of the fundamental diagram approach. No HCT appears regardless of the density, for example, in the NaSch CA model [30] or in the Krauß model [33]: beginning from the critical density $\rho_{cr}^{(J)}$, all states of congested traffic at the fundamental diagram in these models are also unstable up to the jam density ρ_{max}.

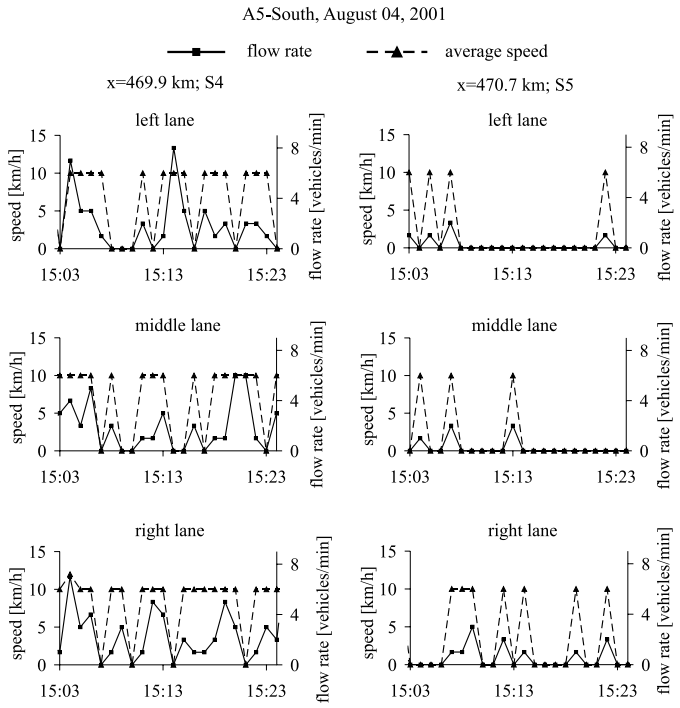

Figure 24. Measured unprocessed flow rate (squares) and speed (triangles) at two detector locations within a congested pattern that has been presented in figure 10(*a*) of [42] as 'homogeneous congested traffic' (HCT). The locations $x = 469.9$ km for the detector S4 and $x = 470.7$ km for the detector S5 are chosen in accordance with the freeway section sketch shown in figure 6 of [42]. The raw data are 1 min averaged data.

In [42, 43] 'empirical' congested traffic states have been published, which should prove the existence of HCT. Based on the measured data processed in [42], let us show that this empirical proof is invalid.

In figure 10 of [42], spatiotemporal speed distributions within two congested patterns are shown to be homogeneous during congested pattern existence. The average speed within the associated patterns is very low, because these patterns have been caused by accidents. It must be stressed that these results of [42] have been derived with an adaptive smoothing method of data processing discussed in [42], i.e., with *processed data sets*. In contrast, our figure 24 shows *real unprocessed raw measured* data for one of these congested patterns related to figure 10(*a*) of [42].

To explain real measured data shown in figure 24, we should note that already in raw unprocessed data there is a large error in the average speed, when very low speeds are measured; if speeds, v, of all vehicles that have passed a detector during a 1 min interval are within the range $0 < v < 20$ km h^{-1}, then the road computer sets the average speed to 10 km h^{-1}. Only if no vehicle passes a detector during a 1 min interval the speed (and flow rate) is zero. This explains why in the speed data shown in figure 24 there are mostly two speed values, zero and 10 km h^{-1}. Only when average speeds are higher than 30 km h^{-1}, the speed can be used in deciding whether the speed distribution is really a homogeneous one or not[6].

[6] This is in contrast with our empirical example shown in figure 22 in which the road computer makes the arithmetical averaging of single-vehicle speeds of vehicles passing a detector during each 1 minute interval. For this reason, in

We see that for low speeds based on the data shown in figure 24, regardless of a method of further speed data processing, *no* conclusion about features of a spatiotemporal pattern can be made from an analysis of speeds *only*, as made in [42]. Rather than the average speed, the flow rate is measured with a sufficient accuracy at any density. We can see from the flow rate distribution shown in figure 24 that there are extremely complex spatiotemporal flow rate changes both in space and time between 0 and 8 vehicles/min/lane. This explains that in contrast with the statement of [42], the congested pattern is extremely non-homogeneous in space and time. Features of such complex spatiotemporal congested patterns occurring at heavy bottlenecks have been found in this paper.

Thus in reality the congested pattern shown in figure 10(*a*) of [42] has no relation with HCT. The same critical conclusion can be made about the congested pattern shown in figure 10(*b*) of [42], which should be another 'empirical' example of HCT.

Due to the existence of HCT model solutions, these traffic flow models exhibit also model solutions called oscillatory congested traffic (OCT) (figure 23(*c*)) [7, 37, 40, 41, 43]. Indeed, OCT appears in a neighborhood of the critical density $\rho_{\rm cr}^{\rm (HCT)}$ for instability of HCT: when the density in HCT decreases and it approaches the critical density $\rho_{\rm cr}^{\rm (HCT)}$, then due to instability of HCT, OCT occurs. Thus OCT model solutions result from the existence of HCT model solutions in these models, i.e., as HCT, OCT model solutions have no relation to real traffic flow.

6.5. Hypothetical driver experiment on circle road associated with traffic congestion conditions at heavy bottlenecks

Here we motivate a driver experiment on a homogeneous circle road without bottlenecks whose results can be compared with some results of the theory of traffic congestion at heavy bottlenecks presented in the paper.

Before we discuss such a hypothetical driver experiment on the circle road at traffic congestion conditions as those occurring at heavy bottlenecks, we should consider simulations of the pinch effect on a single-lane circle road of a length $L_{\rm circle}$, i.e., the spontaneous emergence of wide moving jams in synchronized flow [16]. In an initial homogeneous synchronized flow at a given speed, a local speed disturbance has been applied during a short time interval. Within the disturbance, the decrease in speed is equal to Δv. It has been found [16] that there is a *critical* speed disturbance that amplitude is equal to $\Delta v_{\rm cr}^{\rm (SJ)}$ (figure 25(*a*)). If $\Delta v \geqslant \Delta v_{\rm cr}^{\rm (SJ)}$, then the disturbance grows over time leading to an S $\rightarrow$ J transition; this S $\rightarrow$ J transition occurs only in metastable synchronized flow associated with synchronized flow states that lie on or above the line J in the flow-density plane (figure 18). If in contrast, $\Delta v < \Delta v_{\rm cr}^{\rm (SJ)}$, then the disturbance decays over time. If the density of synchronized flow is great enough, then $\Delta v_{\rm cr}^{\rm (SJ)} \rightarrow 0$ (figure 25(*a*)).

This means that in such an initially homogeneous synchronized flow on a circle road without bottlenecks pinch effect conditions are satisfied, which are qualitatively the same as those in figure 2(*a*), (*b*) upstream of the bottleneck: already small speed (density) disturbances, which occur spontaneously in synchronized flow due to model fluctuations, grow propagating upstream with the subsequent spontaneous emergence of a wide moving jam [16, 44] (figure 25(*b*), (*c*)). This result of three-phase traffic theory [12, 16, 35, 44] has recently been confirmed in a driver experiment [45]. In this experiment, $N_{\rm veh} = 22$ vehicles have initially nearly homogeneously moved along a single-lane circle road with $L_{\rm circle} = 230$ m at speed of about 30 km h^{-1}. Over time, growing local speed (density) disturbances occurred in

figure 22 the speed can be used in deciding made in section 6.3 that the speed distribution is extremely non-homogeneous in space and time.

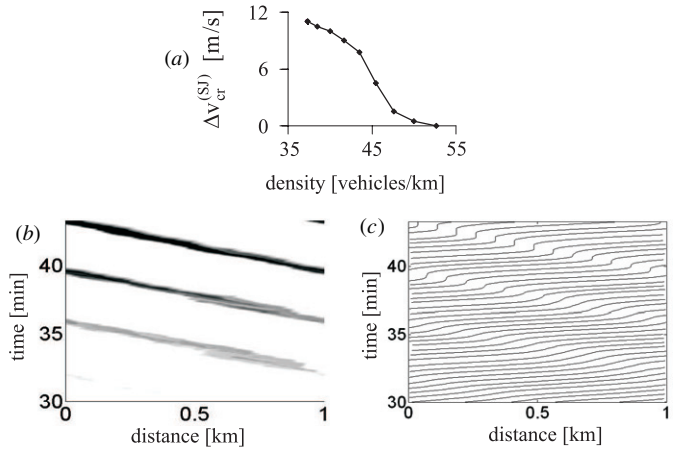

Figure 25. Simulations of the emergence of wide moving jams in synchronized flow on circle road: (*a*) $\Delta v_{cr}^{(SJ)}$ as a function of the density $\rho = N_{veh}/L_{circle}$ at initial synchronized flow speed 40 km h^{-1} (for a comparison, $v_{free} = 108$ km h^{-1}), $L_{circle} = 20$ km. ((*b*), (*c*)) Single-vehicle speed data (*b*) and associated vehicle trajectories (for each tenth vehicle) (*c*) showing the spontaneous emergence of wide moving jam in synchronized flow in space and time at $N_{veh} = 48$ vehicles, $L_{circle} = 1$ km; vehicles start to move from a vehicle standstill at $t = 0$; resulting flow rate $q^{(cong)} = 1210$ vehicles/h. In (*b*) single-vehicle speed data are presented by regions with variable darkness (the lower the speed, the darker the region; in white regions the speed is higher than 20 km h^{-1}). Single-lane model (7)–(25) without bottlenecks with cyclic boundary conditions.

this vehicle motion. The growth of these disturbances led to the formation of a wide moving jam(s) propagating upstream[7].

Qualitatively the same traffic congestion conditions as those occurring at heavy bottlenecks shown in figure 2(*c*), (*d*) can be simulated on the single-lane circle road without bottlenecks, if we now gradually increase the initial vehicle density on the circle road in comparison with pinch effect conditions shown in figure 25(*b*), (*c*). These simulations are presented in figure 26. For the average flow rates $q^{(cong)} \approx 440$ vehicles/h (figure 26(*a*)) and 220 vehicles/h (figure 26(*c*)) in congested traffic on the circle road, which satisfy condition (32), we find qualitatively similar non-regular jam dynamics as those for the same values of $q^{(cong)}$ at heavy bottlenecks (compare figure 26(*a*) with figure 11 and figure 26(*c*) with figure 12). Similarly, for the flow rate $q^{(cong)} \approx 110$ vehicles/h in congested traffic on the circle road that satisfies condition (34) we find a non-regular mega-jam dynamics (compare figure 26(*e*) with figure 15).

In sections 4.3 and 5, we have found that the complexity of the jam dynamics or the mega-jam dynamics becomes the weaker, the more the distance upstream of the bottleneck (figures 13 and 15). It can be assumed that the longer flow interruption intervals and moving blanks propagate on a road, the less the degree of non-regularity in the dynamics of the

[7] The experiment [45] is a very interesting and important one for a deeper understanding of moving jam emergence in synchronized flow. However, both the statement of [45] that the spontaneous moving jam emergence occurs in *free flow* as well as the associated physical explanation of the jam emergence are *invalid*. Indeed, in the experiment vehicles could not overtake each other and the vehicle speed (30 km h^{-1}) has been considerably lower than the speed in free flow (usually higher than 80 km h^{-1} for passenger cars). Moreover, the initial density of the initially traffic flow was $\rho = N_{veh}/L_{circle} \approx 95$ vehicles/km that is considerably greater than the maximal density observed in free flow, which is usually appreciably smaller than 40 vehicles/km/lane. Therefore, rather than free flow, the initial traffic in the experiment of [45] is *congested traffic associated with the synchronized flow phase* as that in simulations presented in figure 25 [16]. Thus as in simulations (figure 25) [16], in driver experiment [45] the spontaneous emergence of wide moving jam(s) in initial synchronized flow (S → J transition) is observed.

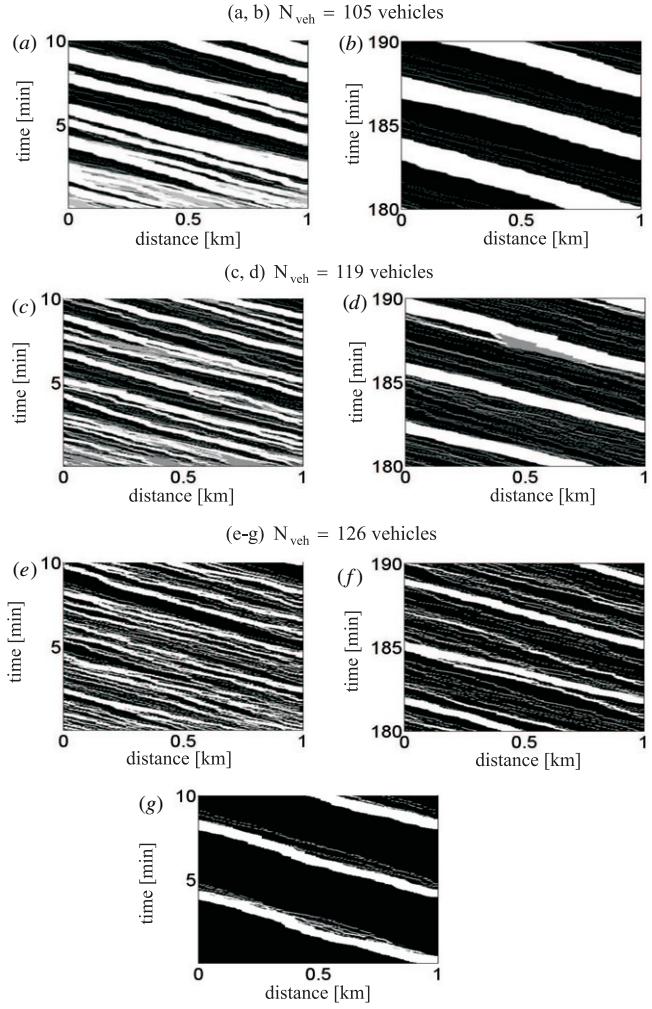

Figure 26. Simulated single-vehicle speed data within wide moving jams (*a*)–(*d*) and mega-jam ((*e*), (*f*)) on circle road of length $L_{\text{circle}} = 1$ km presented in space and time by regions with variable darkness (the lower the speed, the darker the region). White regions (single-vehicle speeds higher than 5.4 ((*a*), (*b*)), 3.6 ((*c*), (*d*)) and 1.8 km h^{-1} (*e*)–(*g*)) are related to synchronized flows between the jams or moving blanks; black regions (single-vehicle speeds are equal to zero) are related to flow interruption intervals. $N_{\text{veh}} = 105$ ((*a*), (*b*)), 119 ((*c*), (*d*)), 126 (*e*)–(*g*). Resulting average flow rate $q^{(\text{cong})} \approx 440$ ((*a*), (*b*)), 220 ((*c*), (*d*)), 110 vehicles/h (*e*)–(*g*). In all simulations, vehicles start to move from a vehicle standstill at $t = 0$. With the exception of figure (*g*), initial (at $t = 0$) space gaps between all vehicles are equal to each other; in contrast with (*e*), in (*g*) at $t = 0$ there is a blank only between two vehicles, whereas initial space gaps between all other vehicles are equal to zero. Other model parameters are the same as those in figure 25.

jams and the mega-jam. This result we indeed find for both the jam dynamics and the mega-jam dynamics on the circle road (see figures 26(*b*), (*d*), (*f*) presenting, respectively, the development of the congested patterns shown in figures 26(*a*), (*c*), (*e*) after 180 min propagation of the patterns on the circle road). In particular, the non-regular dynamics of wide moving jams shown in figures 26(*a*), (*c*) become almost regular ones after wide moving jams propagate during 180 min on the road (figures 26(*b*), (*d*)).

Thus we can expect that some of the spatiotemporal traffic phenomena in congested traffic at a heavy bottleneck (sections 3–5) can also be found in a driver experiment on a circle road without bottlenecks, if in the experiment the initial vehicle density increases leading to the decrease in the average flow rate $q^{(\mathrm{cong})}$ in congested traffic on the road associated with values of $q^{(\mathrm{cong})}$ in traffic congestion at heavy bottlenecks.

However, an emergent congested pattern on the circle road can qualitatively depend on an initial distribution of space gaps between vehicles. An example is shown in figures 26(*e*), (*g*): at the same average density $\rho = N_{\mathrm{veh}}/L_{\mathrm{circle}} = 126$ vehicles/km depending on chosen initial distributions of space gaps between vehicles we find either a non-regular mega-jam dynamics (figure 26(*e*)) or a regular upstream propagation of a single region of moving blanks (figure 26(*g*)). Thus it can assumed that for an adequate comparison of congested patterns at heavy bottlenecks with congested patterns on a circle road without bottlenecks, a nearly homogeneous initial distribution of space gaps between vehicles on the circle road should be chosen.

6.6. Conclusions

Based on a study of traffic congestion with the Kerner–Klenov stochastic three-phase traffic flow model and a heavy bottleneck model presented in the paper, we can make the following conclusions:

(1) When the bottleneck strength, i.e., the influence of a bottleneck on traffic is not very great, then traffic breakdown at the bottleneck occurring at large enough flow rates upstream of the bottleneck results in a well-known general congested pattern (GP) [12]. As in empirical GPs, in simulations the GP consists of the pinch region of synchronized flow in which narrow moving jams emerge and grow propagating upstream; at a upstream boundary of the pinch region, some (or sometimes all) of the jams transform into wide moving jams, i.e., a sequence of the wide moving jams propagating upstream is realized. When the bottleneck strength increases, then GP parameters change as earlier found in theoretical studies of GPs occurring at various bottlenecks [12]: the average flow rate in the pinch region and the mean pinch region width (in the longitudinal direction) decrease, the frequency of the jams increases, the average speed between wide moving jams decreases. However, we found that this regular spatiotemporal structure of the GP remains at the bottleneck only, if the bottleneck strength does not exceed some critical value.

(2) When the bottleneck strength increases further and it exceeds a critical bottleneck strength, features of traffic congestion at such a heavy bottleneck change qualitatively. A pinch region of synchronized flow within the GP disappears and appears randomly over time: an GP with a non-regular pinch region appears at the bottleneck. The more the bottleneck strength exceeds the critical bottleneck strength, the longer the mean duration of random time intervals within which the regular structure of the GP breaks and the pinch region disappears, and therefore, the smaller the mean width of the pinch region.

(3) There is a threshold bottleneck strength for the pinch region existence at which the pinch region of a GP dissolves fully: at this and greater bottleneck strengths, the GP without pinch region is formed, i.e., it consists of a sequence of wide moving jams, all of them emerge directly at the upstream boundary of the heavy bottleneck.

(4) Wide moving jams of GPs with a non-regular pinch region and without pinch region can exhibit a very complex and non-regular spatiotemporal dynamics. The jam dynamics is associated with the effects of the emergence, splitting, dissolution and merging of flow interruption intervals, which occur randomly within a sequence of wide moving jams.

(5) The complex non-regular dynamics of traffic congestion of items 2–4 is explained by a competition between the random nucleation of moving jams in metastable synchronized flow and the random jam dissolution incorporated in the stochastic traffic flow model of section 2.1 through the use of the speed adaptation in synchronized flow as well as random time delays in driver acceleration and deceleration. As a result, simulations of the model show that the greater the density in synchronized flows of the pinch region and between wide moving jams upstream of the pinch region, the smaller the critical speed disturbance (the smaller the nucleus) required for the moving jam nucleation, and consequently the smaller the mean time delay of the jam nucleation. The density in the synchronized flow increases with the increase in the bottleneck strength. The time delay of the jam nucleation is a random value. When the bottleneck strength increases, the mean time delay of the jam nucleation becomes a small enough value and therefore there are random time intervals, when time delays of the jam nucleation are negligible: wide moving jams emerge directly upstream of the bottleneck, i.e., the pinch region disappears. During other random time intervals, when time delays of the jam nucleation are great enough, the pinch region appears again. The subsequent increase in the bottleneck strength causes the decrease in the mean time delay of the jam nucleation up to zero; as a result, all wide moving jams emerge almost directly upstream of the bottleneck and the pinch region disappears fully.

Simulations show that the similar random effect of wide moving jam nucleation occurs in synchronized flow between wide moving jams. However, in comparison with synchronized flows between wide moving jams propagating on a homogenous road upstream of the bottleneck, there is an addition source of random speed fluctuations in a neighborhood of the bottleneck caused by a longer safety time headway within the bottleneck. This can explain why a non-regular pinch region appears at the bottleneck at smaller bottleneck strengths than those required for the random jam nucleation in synchronized flows between wide moving jams propagating on the homogeneous road far away upstream of the bottleneck.

(6) There is also another critical bottleneck strength called the critical bottleneck strength for the mega-jam formation, which is greater than the threshold bottleneck strength at which the pinch region of a GP dissolves fully (item 3). When the bottleneck strength exceeds the critical bottleneck strength for the mega-jam formation, wide moving jams of the GP merge onto a mega-wide moving jam (mega-jam). The microscopic structure of a mega-jam consists of alternating regions of flow interruption intervals and moving blanks propagating upstream within the mega-jam. When wide moving jams merge onto the mega-jam, traffic congestion upstream of the bottleneck cannot be considered as a GP any more. The time-functions of average speed within the mega-jam exhibit a non-regular behavior.

The merger of wide moving jams onto the mega-jam is realized when the average flow rate in traffic congestion upstream of the bottleneck becomes as small as the average flow rate of low-speed states associated with moving blanks within wide moving jams. In this case, the difference between flows within and outside wide moving jams disappears; as a result, wide moving jams should merge into the mega-jam.

(7) The microscopic structure of the mega-jam exhibits complex dynamics of alternating regions of flow interruption intervals and moving blanks over time, i.e., during their upstream propagation within the mega-jam. These effects can be explained by great fluctuations of moving blanks and flow interruption intervals occurring during their upstream propagation. These fluctuations are associated with lane changing as well as with random time delays in vehicle acceleration and deceleration, which can make a

great influence on a random low-speed vehicle motion resulting in moving blanks within the jam. Moreover, a random time delay in vehicle acceleration from a vehicle standstill within a flow interruption interval can cause fluctuations in the velocity of the downstream front of the flow interruption interval.

(8) Results of items 1–7 allow us to conclude that the evolution of the traffic phases in congested traffic, when heavy bottlenecks caused for example by bad weather conditions or accidents occur in highway traffic, is as follows. The greater the bottleneck strength, i.e., the smaller the average flow rate allowed by the heavy bottleneck within the congestion, the less the mean pinch region width (items 2 and 3). When the bottleneck strength increases further strongly and it reaches the critical bottleneck strength for the mega-jam formation (item 6), the pinch region does not exist and only the mega-jam survives and synchronized flow remains only within its downstream front separating free flow and congested traffic. Thus a congested pattern at such a very heavy bottleneck consists of synchronized flow within the downstream front of the pattern and the mega-jam upstream of the bottleneck.

(9) The characteristic spatiotemporal traffic phenomena of items 1–8, in particular the occurrence of a GP with a non-regular pinch region, the non-regular jam dynamics, and the mega-jam formation should occur when the average flow rate $q^{(\mathrm{cong})}$ in congested traffic reaches small enough values. We can expect that the flow rate $q^{(\mathrm{cong})}$ characterizes the bottleneck strength regardless of the cause of a bottleneck. Therefore, the characteristic traffic phenomena found in the paper (items 1–8) should be expected upstream of any heavy bottleneck or bottleneck sequence at small enough values of $q^{(\mathrm{cong})}$.[8]

(10) Results of a theory of traffic congestion at heavy bottlenecks (items 1–8) presented in the paper can qualitatively explain why sequences of wide moving jams, which are observed in 1 min average measured data of congested patterns at usual bottlenecks, are not observed in measured average data of non-homogeneous congested traffic occurring at very heavy bottlenecks caused for example by bad weather conditions or accidents.

Acknowledgments

I thank Sergey Klenov for help in simulations, Ines Maiwald-Hiller for help in data analysis, Andreas Hiller, Gerhard Nöcker, Hubert Rehborn and Olivia Brickley for suggestions. I thank also the authorities of the Federal State Hessen in Germany that made available unprocessed raw measured data.

References

[1] May A D 1990 *Traffic Flow Fundamentals* (Englewood Cliffs, NJ: Prentice-Hall)
[2] Leutzbach W 1988 *Introduction to the Theory of Traffic Flow* (Berlin: Springer)
[3] Gartner N H, Messer C J and Rathi A (ed) 1997 *Special Report 165: Revised Monograph on Traffic Flow Theory* (Washington, DC: Transportation Research Board)
[4] Daganzo C F 1997 *Fundamentals of Transportation and Traffic Operations* (New York: Elsevier)
[5] Gazis D C 2002 *Traffic Theory* (Berlin: Springer)
[6] Chowdhury D, Santen L and Schadschneider A 2000 *Phys. Rep.* **329** 199
[7] Helbing D 2001 *Rev. Mod. Phys.* **73** 1067–141

[8] In real highway networks, there can often be a sequence of two or more very close located adjacent bottlenecks (for example, on- and off-ramp bottlenecks, bottlenecks due to lane reduction, etc) limiting the flow rate $q^{(\mathrm{cong})}$ upstream of the farthest upstream bottleneck of the bottleneck sequence to values that can satisfy (6). Thus upstream of the bottleneck sequence qualitatively the same phenomena in congested traffic should occur as those at an isolated heavy bottleneck (items 1–8).

[8] Nagatani T 2002 *Rep. Prog. Phys.* **65** 1331–86
[9] Nagel K, Wagner P and Woesler R 2003 *Oper. Res.* **51** 681–716
[10] Mahnke R, Kaupužs J and Lubashevsky I 2005 *Phys. Rep.* **408** 1–130
[11] Maerivoet S and De Moor B 2005 *Phys. Rep.* **419** 1–64
[12] Kerner B S 2004 *The Physics of Traffic* (Berlin: Springer)
[13] Kerner B S, Klenov S L and Hiller A 2006 *J. Phys. A: Math. Gen.* **39** 2001–20
[14] Kerner B S, Klenov S L, Hiller A and Rehborn H 2006 *Phys. Rev.* E **73** 046107
[15] Kerner B S and Klenov S L 2006 *J. Phys. A: Math. Gen.* **39** 1775–809
[16] Kerner B S and Klenov S L 2002 *J. Phys. A: Math. Gen.* **35** L31–43
[17] Kerner B S, Klenov S L and Wolf D E 2002 *J. Phys. A: Math. Gen.* **35** 9971–10013
[18] Davis L C 2004 *Phys. Rev.* E **69** 016108
[19] Lee H K, Barlović R, Schreckenberg M and Kim D 2004 *Phys. Rev. Lett.* **92** 238702
[20] Jiang R and Wu Q-S 2004 *J. Phys. A: Math. Gen.* **37** 8197–213
[21] Gao K, Jiang R, Hu S-X, Wang B-H and Wu Q-S 2007 *Phys. Rev.* E **76**
[22] Laval J A 2007 *Traffic and Granular Flow '05* ed A Schadschneider, T Pöschel, R Kühne, M Schreckenberg and D E Wolf (Berlin: Springer) pp 521–6
[23] Davis L C 2006 *Phys.* A **368** 541–50
Davis L C 2006 *Phys.* A **361** 606–18
Davis L C 2007 *Phys.* A **379** 274–90
[24] Jiang R, Hua M-B, Wang R and Wu Q-S 2007 *Phys. Lett.* A **365** 6–9
[25] Jiang R and Wu Q S 2005 *Phys. Rev.* E **72** 067103
Jiang R and Wu Q S 2007 *Phys.* A **377** 633–40
[26] Wang R, Jiang R, Wu Q S and Liu M 2007 *Phys.* A **378** 475–84
[27] Pottmeier A, Thiemann C, Schadschneider A and Schreckenberg M 2007 *Traffic and Granular Flow' 05 Proc. of the International Workshop on Traffic and Granular Flow* ed A Schadschneider, T Pöschel, R Kühne, M Schreckenberg and D E Wolf (Berlin: Springer) pp 503–8
[28] Li X G, Gao Z Y, Li K P and Zhao X M 2007 *Phys. Rev.* E **76** 016110
[29] Kerner B S and Klenov S L 2003 *Phys. Rev.* E **68** 036130
[30] Nagel K and Schreckenberg M 1992 *J. Phys. (France) I* **2** 2221–9
[31] Gazis D C, Herman R and Rothery R W 1961 *Oper. Res.* **9** 545–67
[32] Barlović R, Santen L, Schadschneider A and Schreckenberg M 1998 *Eur. Phys. J.* B **5** 793–800
[33] Krauß S, Wagner P and Gawron C 1997 *Phys. Rev.* E **55** 5597–602
[34] Gipps P G 1981 *Trans. Res.* B **15** 105–11
[35] Kerner B S 1998 *Phys. Rev. Lett.* **81** 3797–400
Kerner B S 1998 *Proc. 3rd Symposium on Highway Capacity and Level of Service Road Directorate, Ministry of Transport, Denmark* vol 2 ed R Rysgaard pp 621–42
Kerner B S 1999 *Trans. Res. Rec.* **1678** 160–7
[36] Kerner B S and Konhäuser P 1994 *Phys. Rev.* E **50** 54–83
[37] Lee H Y, Lee H-W and Kim D 1999 *Phys. Rev.* E **59** 5101–11
[38] Tanga C F, Jiang R and Wu Q S 2007 *Phys.* A **377** 641–50
[39] Bando M, Hasebe K, Nakayama A, Shibata A and Sugiyama Y 1994 *Japan. J. Appl. Math.* **11** 203–23
Bando M, Hasebe K, Nakayama A, Shibata A and Sugiyama Y 1995 *Phys. Rev.* E **51** 1035–42
Bando M, Hasebe K, Nakayama A, Shibata A and Sugiyama Y 1995 *J. Phys. I (France)* **5** 1389–99
[40] Berg P and Woods A 2001 *Phys. Rev.* E **64** 035602
[41] Helbing D, Hennecke A and Treiber M 1999 *Phys. Rev. Lett.* **82** 4360–3
[42] Schönhof M and Helbing D 2007 *Transp. Sc.* **41** 135–66
[43] Treiber M, Hennecke A and Helbing D 2000 *Phys. Rev.* E **62** 1805–24
[44] Kerner B S 1999 *Transportation and Traffic Theory* ed A Ceder (Amsterdam: Elsevier) pp 147–71
[45] Sugiyama Y, Fukui M, Kikuchi M, Hasebe K, Nakayama A, Nishinari K, Tadaki S and Yukawa S 2008 *New J. Phys.* **10** 033001

J. Phys. A: Math. Theor. **41** (2008) 369801 (1p) doi:10.1088/1751-8113/41/36/369801

Corrigendum

A theory of traffic congestion at heavy bottlenecks
Boris S Kerner 2008 *J. Phys. A: Math. Theor.* **41** 215101

The first sentence in the caption of figure 15, 'Fragments of figure 10(*d*) in larger scales in the left (figures left) and right lanes (right)' should be replaced by 'Simulated single-vehicle speed data within a mega-jam presented in space and time by regions with variable darkness (the lower the speed, the darker the region). Left and right figures are related to the left and right lanes, respectively'.

1751-8113/08/369801+01$30.00